NEAR INFRARED SPECTROSCOPIC ASSESSMENT OF BONE WATER BINDING TO COLLAGEN AND MINERAL

A Dissertation
Submitted to
Temple University Graduate Board

In Partial Fulfillment
of the Requirements for the Degree
DOCTOR OF PHILOSOPHY

---

by
Ramyasri Ailavajhala
May 2019

Examining Committee Members:

Nancy Pleshko, Ph.D., Thesis Advisor, Bioengineering
Chetan Patil, Ph.D., Bioengineering
Mary Barbe, Ph.D., Department of Anatomy and Cell Biology
Allison Tumarkin-Deratzian, Ph.D., Earth and Environmental Sciences
Chamith Rajapakse, Ph.D., Departments of Radiology and Orthopedic Surgery, University of Pennsylvania

ABSTRACT

Cortical bone fragility increases with age, therapeutic drug use and disease states. Clinically, bone fragility is evaluated by assessment of bone mineral density (BMD); however, studies have shown that other factors such as bone architecture, cell turnover and tissue composition influence bone quality. There is growing evidence that age related changes in bone water associated with collagen and/or mineral have a direct impact on bone mechanical competence and structural integrity. Understanding these compositional changes will aid in improved diagnose and prediction of fractures.

Magnetic resonance imaging (MRI) is used to evaluate bone water, but this modality is limited in spatial resolution and is still being developed. Although still in the experimental stage, vibrational spectroscopy in the near infrared region (NIR) also known as near infrared spectroscopy (NIRS) is a nondestructive modality that can spatially evaluate alterations of bone composition.

NIRS is a unique nondestructive technique that produces a signature spectrum by penetrating high frequency (4000-12,000 cm^{-1}) non-ionizing radiation into material. NIRS permits a depth of penetration from millimeters to centimeters, dependent on frequency (wavelength). NIRS is very sensitive to water and can be used to provide molecular information of water related to collagen and mineral in bone samples. To date, definitive information on which NIR absorbances are linked to collagen or mineral bound water have not been identified.

The overarching hypothesis is that water associated with collagen and/or mineral can be identified using NIRS and will serve as a biomarker for bone fragility in future

preclinical studies. This will be achieved with the following three aims: First, to develop a method to image human cortical bone tissue using NIRS; second, to identify NIRS absorbances of water bound with mineral and collagen in bone; and finally, the third aim, to correlate the NIRS-derived water content in human cortical bone to structural properties determined by micro-computed tomography (micro-CT). Together these studies will establish the NIRS technique as a powerful tool to screen and monitor aging and diseased tissues in preclinical studies.

DEDICATION

To My Parents

(Raghuram and Padmaja Ailavajhala)

&

To My Inspiration, My Brother

Mahesh Satyanarayana Ailavajhala, Ph.D.

ACKNOWLEDGMENTS

This work was completed in tissue imaging spectroscopy lab (TISL), Department of Bioengineering, Temple University, during the years of 2013-2019. This study has been supported by National Institutes of Health (NIH).

I would like to sincerely thank my advisor Dr. Nancy Pleshko, for her support, guidance and encouragement throughout my graduate school at Temple University. I have been privileged to have her as my advisor. I would like to thank her for being a positive mentor to me and everyone in the Department of Bioengineering.

I would also like to convey my gratitude towards my examining committee members, Dr. Patil, Dr. Barbe, Dr. Deratzian and Dr. Rajapakse for their guidance. I would like to thank Dr. Rajapakse for supporting me throughout my graduate research. I would like to acknowledge Dr. Barbe for always willing to answer my questions and encouraging me in the last year. I would like to thank Dr. Patil for his excellent inputs. I would like to acknowledge, Dr. Deratzian for willing to be an external examiner for my defense.

I would like to express my deepest gratitude and thanks to all current and former TISL members. I would not have been able to come this far in my graduate school journey without the support from everyone. I would like to thank Jack Oswald and Dr. William Querido for all your help and encouragement.

To Jessica Falcon and Shital Kandel, thank you for being my strength and support system each and every day. I am very fortunate to have both of you in my life.

I would like to acknowledge Mrs. Helen Freitas and Mrs. Doreen Aiello for helping me and everyone in department of bioengineering.

To my childhood friend Roxanna Abbasi, your support has been vital for me throughout my life. I could not have asked for a better best friend and confidant.

To my parents, Raghuram and Padmaja Ailavajhala, thank you for your love, support and encouragement. You have made it possible for me to pursue this degree and I am so lucky to be your daughter.

To my brother, you are my inspiration and my strength thank you for always being by my side.

Ramyasri Ailavajhala April 2019

Table of Contents

LIST OF FIGURES

LIST OF TABLES

CHAPTER 1: INTRODUCTION

1.1 Bone composition

Cortical bone is a tri phasic heterogeneous tissue consisting of approximately 25% collagen fibrils, 65% mineral crystals and 10% water [1]. The relative proportions of each component change depending on various factors, primarily age, sex and disease. The individual components of bone serve as building blocks to form a compact structure that protects marrow and spongy bone. As shown in Figure 1, cortical bone is organized in a hierarchal manner that optimizes the ability to provide rapid repair, growth of bone tissue during fracture healing and to easily adjust to changing mechanical needs to provide stability and strength for the body [2-4].

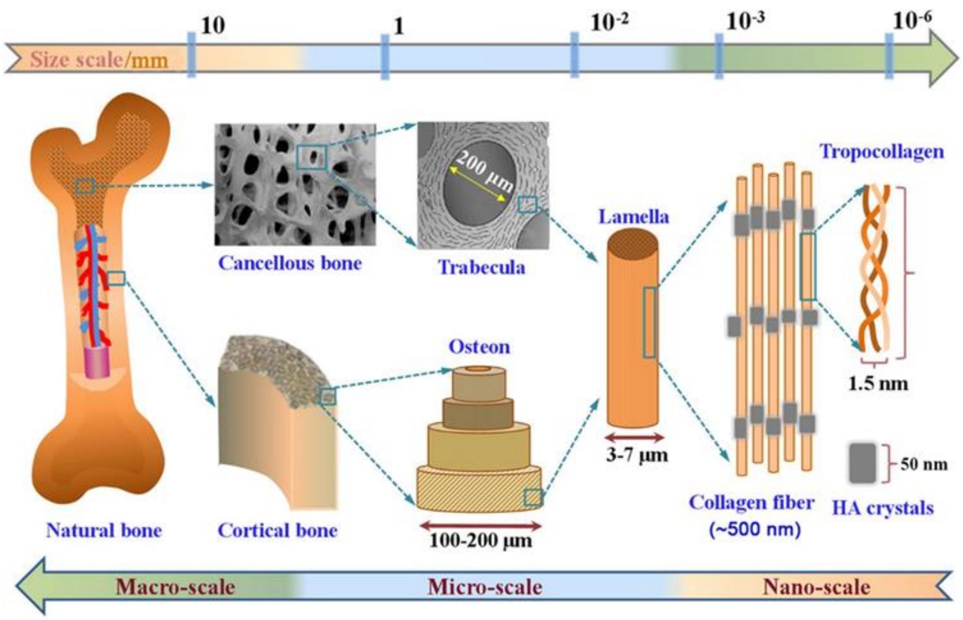

Figure 1: Hierarchical image of bone from macro to nano-scale [4].

Collagen

Type 1 collagen consists of approximately 90% of the organic matrix in bone tissue [5]. Collagen fibrils form from tropocollagen, a triple helical structure that comprises of alpha 1 & two identical alpha 2 chains [6,7]. Each collagen chain is approximately composed of 1000 amino acids in length and consists of repeating sequence of amino acids (Gly-X-Y) glycine positioned at every third residue, (X) proline in the central position and (Y) hydroxyproline (the post-enzymatic translation of proline). The ends of the alpha chains consist of either a carboxyl (COOH-) group or an amino functional (-NH2) group. Together the three chains are intertwined to form the right-hand triple helical structure known as collagen. In length and diameter collagen is approximately 300 nm and 1.5 nm respectively. As shown in Figure 2, collagens molecule are aligned adjacent to each other with an approximate offset of D =67 nm in the parallel direction to form fibrils, which then aggregate to create a bundle [8]. Covalent crosslinking helps to join fibrils together to render a compact collagen bundle. The precisely formed triple helical structure of collagen acts as a scaffold for mineral and water deposition.

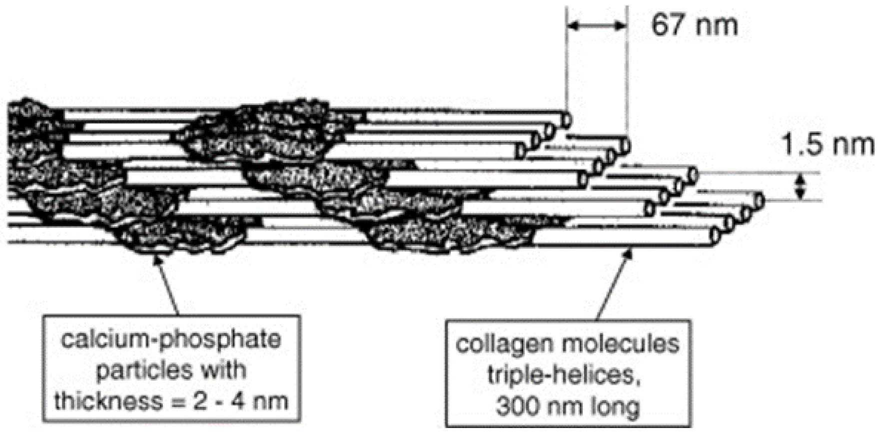

Figure 2: Mineralized Collagen Fibrils compacted to create a collagen bundle [8].

Non-collagenous Proteins

Approximately 5 % of the organic matrix of bone consists of non-collagenous proteins (NCP) such as osteopontin, sialoprotein, osteonectin, osteocalcin, fibronectin [9]. These proteins help to regulate the size, the orientation and the amount of mineral deposition along the collagen fibrils [10,11].

Mineral

Hydroxyapatite is the primary mineral constituent in bone, $Ca_5(PO_4)_3(OH)$, and is found as a poorly crystalline and carbonated phase [3,12,13]. In apatite carbonate often substitutes either for OH or PO_4 [14]. Initially, amorphous calcium phosphate and carbonate nucleate in between gaps of collagen fibrils and spread throughout the organic matrix. As the bone matures, the carbonate content is reduced, mineral crystals form and grow along the collagen fibrils, with typical thickness ranging from 2 to 4 nm [8]. The newly mineralized organic bundles have increased mechanical competence; the inherent toughness of bone originates from crosslinking of collagen fibers, while the mineral deposition provides increased compressional strength.

Water

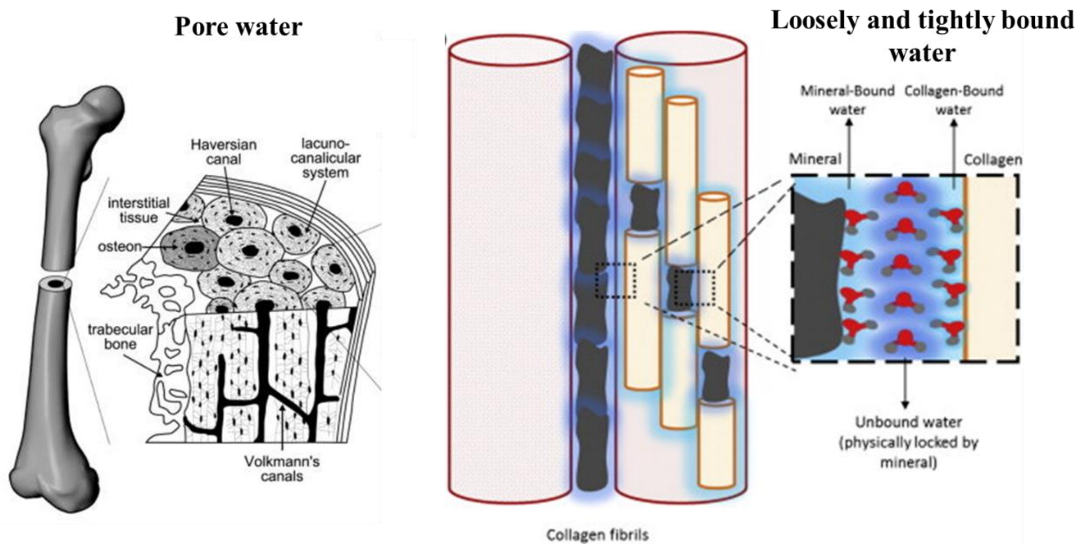

Figure 3: Location of pore[15], *loosely and tightly bound water in cortical bone* [16].

Water can be found in different environments in the hierarchal organization of cortical bone. As seen in Figure 3, the three commonly reported forms of cortical bone water are free, loosely (surface) and tightly bound [15,16]. Free water is located within the macroscopic pores and within the microscopic pores of the haversian canal and lacuna-canalicular system [15]. Free water contributes to the viscoelastic properties of bone and aids in nutrient exchange within the haversian canals [15]. Loosely bound water is found either in between the collagen and the mineral interphase, or hydrogen bound to exposed surfaces of collagen and mineral, whereas, tightly bound water is described as water located within the structure of either collagen or mineral. Loosely and tightly bound water in bone provides structural stability and mechanical integrity.

Collagen-Associated water

The interaction between hydroxyproline amino acids and water plays a crucial role in stabilizing collagen's helical structure via intra & inter molecular hydrogen bonding. The water bridges created between the hydroxyl group of the amino acid and the water molecules helps to stabilize a single collagen fiber via intramolecular bonding [17]. The hydrogen bonding between water molecules and the polar hydrophilic side chains of collagen helps to bind adjacent fibrils through intermolecular bonding.

Mineral-Associated water

There are two main water compartments that are associated with bone mineral; one being loosely bound water found at the surface of mineralized collagen fibrils, and the second being tightly bound water residing within the apatite crystal lattice structure. The tightly bound water molecules help to stabilize the local mineral structure by creating bridges via hydrogen bonding of water to the surrounding ions in the hydroxyapatite. Generally, most of the water in bone is collagen bound and only a small portion is mineral associated water[18]; nevertheless, the type and amount of water found in bone depends on factors such as age, sex and tissue composition.

1.2 Bone Quality Assessment

Age and disease states tend to change and impact the overall bone quality in skeletal tissue. Osteoporosis, a disease of the bone, affects approximately 53 million men and women in the United States, most of whom are above the age of 50 years [19]. It results in a decrease in bone mass and increase in bone porosity. Clinically, bone mineral density (BMD) measurements are conventionally used for assessing bone quality [20-22].

BMD is measured through dual X-ray absorptiometry (DXA), a technique that requires ionizing radiation. DXA-derived parameters are used to distinguish normal versus diseased (primarily osteoporotic) tissues. BMD scores reflect the amount of bone tissue based on the mass of mineral over a known tissue area. Osteoporosis is defined by BMD score of -2.5 standard deviations lower than the average bone mass of healthy adults [22]. BMD values are described in terms of T-scores, which indicate the deviation of a measured bone mass from the BMD values of the average bone mass. In other words, T-score is expressed as a standard deviation, and it is a value that shows the variance between the measured bone mass to the bone mass of a healthy 30-year-old individual. Z-score, on the other hand, compares the measured BMD values of one individual to BMD values of others that are similar in age and sex. In most clinical settings T-score is most often used to indicate if a patient has normal or osteoporotic tissue.

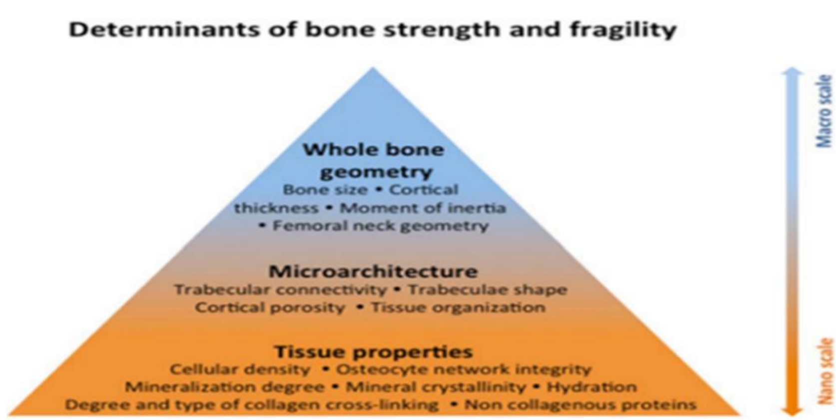

Figure 4: Several factors such as bone geometry, architecture and tissue properties affect bone quality at every scale [22].

Bone quality is a reflection of bone strength and fragility. As indicated in Figure 4,[22] several factors in addition to BMD influence bone quality. For example, variation in compositional components play a key role in the overall structural changes in bone [22]. Studies have shown that BMD alone is not the sole indicator for fracture risk. A review paper by Khan et al.[23], suggested that bone mass values in a population resemble a bell curve, and 15 percent of healthy women have low bone density throughout their life. Upon reaching premenopausal age these women might be diagnosed with osteoporosis according to BMD standards [23]. This could be an inaccurate diagnosis, as a low BMD at premenopausal age does not necessarily result in osteoporosis, as other factors should be considered alongside BMD such as microdamage to the skeletal tissue or any compositional changes due to age. Several review papers have highlighted that BMD as an indicator for bone quality leads to under or over predictions for risk of fracture [21-25]. The misdiagnosis of osteoporosis can be harmful for prescribing therapeutics to patients. Therefore, it is important to develop methods and evaluate reliable biomarkers for skeletal fragility. One such marker may be bone water. The gradual decrease of bone water during aging has the potential to be utilized as a tool to predict bone quality [26, 27].

1.3 Age Related Changes in Water Binding to Collagen and Mineral

Aging is associated with a decrease in bone mass and increased fragility [1]. Bone has the innate ability to repair and remodel its mineralized organic matrix through a dynamic process of resorbing and rebuilding by osteoclast and osteoblast cells, respectively [28]. Bone loss that precedes osteoporosis is triggered by increased cellular activation of osteogenic remodeling. This remodeling yields an imbalance between bone resorption and reformation. Although the degree and process of remodeling in aging tissue is not well understood, the degree of mineralization is greater in older samples due to a one to one exchange of water molecules with mineral crystals [28]. With time, this exchange causes a reduction in water content and increase in bone stiffness. Interestingly, aging is also thought to initiate an increase in displacement of collagen-associated water due to increased glycated cross-linking in collagen fibrils [27, 29, 30]. The slow dehydration of bone overtime increases collagen stiffness, consequently causing an increase in bone brittleness and reduction in skeletal toughness. Understanding the correlation between bone water content and aging could provide insight into the overall bone quality.

1.4 Therapeutics that Reduce Age-Related Water Loss

Most humans reach peak bone mass by the age of 30, which is the point at which bone tissue is considered to have maximum strength and mineral density [31]. After the age of 50 premenopausal symptoms trigger changes in estrogen levels causing rapid bone loss due to increased tissue resorption [31, 32]. Continuous loss of bone after menopause can lead to osteoporosis, which affects more than half of the female and 1/5 of the male populations [33].

Antiresorptive drugs are commonly prescribed medications to treat low bone mass. The two most common types of antiresorptive drugs are bisphosphonates and selective estrogen receptor modulators (SERM) [34-36]. Bisphosphonates such as alendronate function by directly attaching to the mineral binding sites designated for osteoclasts on bone tissue during active cell resorption. Additionally, bisphosphonates reduce the number of osteoclasts cells in tissues by inhibiting the recruitment and proliferation of osteoclast progenitor cells. SERM drugs such as raloxifene work to stop bone resorption by having a high affinity to estrogen receptors to control and slow down the remodeling process initiated by osteoclasts [37-41]. Another drug that is important to mention for treating low mass in tissues is Denosumab [36, 42]. This is a human monoclonal antibody that binds to RANKL, a surface receptor on osteoclasts, this drug work by inhibiting the formation, proliferation, function of osteoclasts. Therefore, it actively works to decrease bone resorption in tissues. It is important to note that these drugs help to reduce fracture risk in osteoporotic tissues by stabilizing the rate of bone formation and resorption.

Bisphosphonates help to reduce fracture risk, but have not been shown to affect tissue water [40]. However, studies focused on understanding the effects of raloxifene found that it directly increases tightly bound collagen water [41]. The spacing between collagen fibrils changes with decreased estrogen levels in the body [41]. In raloxifene-treated animals, this spacing increases and water molecules bind to collagen fibrils causing swelling within the collagen structure. The exact mechanism is not fully understood, however, this increased spacing and increased water content improves overall mechanical competence of cortical bone [40, 41]. This further motivates research into understanding water’s role in bone quality assessment for therapeutic advancements.

1.5 Current Methods to Qualitatively and Quantitatively Evaluate Bone Structure and Composition

A conventional technique used to determine water content in skeletal tissues is gravimetric analysis [22]. This method consists of weighing pieces of cortical bone in a natural hydrated state, and when it is dried. The difference in wet and dry sample weights yields the overall water content for the samples. To obtain mineral content, the bone is weighed, and then heated to above 600° Celsius to remove collagen and other organic matter (ashed), and then weighed again. The difference between the two sample weights is then calculated as the mineral weight [25]. The collagen content can be estimated by ashing as previously described, or more precisely determined by a hydroxyproline assay [27, 28]. These approaches provide an insight into overall bulk amount of mineral, collagen and water. The drawbacks to these analyses are that they are time consuming, destructive to the samples, and cannot be used to understand the spatial distribution of the three primary bone components.

Microscopy Techniques for Assessment of Bone Microstructure

Micro-computed tomography (micro-CT) is used to visualize structure and geometry in bone tissues at ~ 3-10-micron spatial resolution. X-rays generated from a source are transmitted through a sample that is rotating by a fraction of a degree at a time on a sample holder, and then sent to a detector for analysis [25]. A series of two-dimensional X-ray projections are reconstructed into three dimensional images. Micro-CT is considered a gold-standard technique for analysis of geometric properties of bone including porosity, volume, tissue and overall bone mineral density [25]. It can take several hours to days to acquire high-resolution three-dimensional images, depending on the size of the sample and resolution of the scans.

The structural and morphological features of bone at the nanoscale have been investigated through techniques such as transmission, scanning and atomic force microscopy. In transmission electron microscopy (TEM) a coherent beam of electrons controlled by an aperture are transmitted through a thin (~2 microns) bone section [43]. The interaction between the sample and the incident electron beam are then analyzed by a charged couple device (CCD) which helps generate to an image. The sample sections must be thin to allow electrons to transmit through the entire section with minimum energy loss. The resolution for TEM can be as a low as 0.2 nm [44], [45]. The sample preparation for TEM is arduous since it requires samples to be fully dehydrated, embedded in resin and then cut into very thin sections for imaging [44]. TEM images helps to reveal nano-scale structural properties such as mineralized collagen fibrils in bone tissues.

Similarly, in scanning electron microscopy (SEM) images are generated by a cone of high energy electrons scanning the surface of the sample. The electrons interact with the atoms in the sample and then produce three main signals, secondary electrons, backscattered electrons and energy dispersive X-rays [43, 45, 46]. Secondary and backscattered electrons are generated by inelastic and elastic collisions between the incident beam and the sample’s electrons respectively. Secondary electrons are lower in energy but produce high resolution images revealing information about the surface of the sample. Whereas, backscattered electrons are penetrated deep within the sample which help to explain atomic level elemental information. Energy dispersive X-rays that are generated can also be used as finger prints of each element within in the sample, for example Calcium to Phosphorus ratio is often calculated to determine the mineral content in the sample [43]. The approximate resolution for SEM is 10 nm [46]. Sample preparation for SEM is a twostep process that involves dehydration followed by polishing and coating the surface of the sample with an electrically conductive material such as gold.

Atomic Force Microscopy (AFM)

Over the past several years AFM has been increasingly used to understand bone's nanostructure properties [47-50]. AFM helps to quantify local mineral crystal size, collagen fibril orientation, diameter and structure [50]. The images are produced by a cantilever attached with a very sharp tip that probes a region on the bone by moving up and down. A signal is generated by a reflecting a laser beam off the cantilever and onto a photo-detector which is then sent to a computer to produce a three-dimensional spatially distributed topographic image. The resolution of AFM images in the z direction is 0.1nm, in the x and y direction it is less than 5 nm [50]. There is little to no sample preparation in AFM; however, since the radius of the cantilever tip is less than 10 nm, collection of an image from a large section of bone is time consuming [50].

Analytical methods such as vibrational spectroscopy and magnetic resonance imaging (MRI) have also been used pre-clinically and clinically (MRI) to evaluate bone water, mineral and collagen content (described below) [20, 27, 51, 52]. These methods are non-destructive, at times non-invasive (MRI), and allow for chemical correlation between two or more components within the same sample.

Magnetic Resonance Imaging (MRI)

MRI is often used to investigate the components of cortical bone tissue because of its sensitivity to proton microenvironments. In MRI, protons inside tissues align according to an applied magnetic field. Radio frequency (RF) waves are then introduced to tissues causing the alignment of protons to be disrupted [53]. The time it takes the protons to return to equilibrium is measured in terms of relaxation times of parameters T_1 and T_2 [53]. The tissues are subjected to consecutive RF pulses, and the time in between each pulse (TR) and the time of the emitted signal (TE) are measured [51, 53, 54]. Ultrashort echo time (UTE)-MRI helps to further explore the relaxation time of T_2 measurements from the various cortical bone water compartments. T_2 relaxation time is the measurement of transverse decay of proton magnetization. Since cortical bone is a dense tissue, tightly bound water's relaxation time is shorter compared to loosely bound water. The detected proton signal theoretically can arise from several constituents of bone (i.e. collagen, mineral and lipids) [16]. The biggest drawback of UTE-MRI is that to date, these methods can it only detect water associated with collagen, since the proton signal from mineral is too short to be detected by this modality [43]. Several studies have used UTE-MRI to quantify cortical bone water content, and in human cadaveric tissues have shown that 60-90% of water is bound to collagen [27]. Additionally, studies in bovine cortical bone have also suggested that ~73% of water that is detected is collagen bound [51]. According to the majority of MRI literature on cortical bone, water that is found in bone is collagen-associated and little information is known regarding mineral bound water.

1.6 Vibrational Spectroscopy

Vibrational spectroscopic techniques such as Raman and Fourier transform spectroscopy, either in bulk or imaging mode (FT infrared (FT-IR) imaging spectroscopy, FT-IRIS), are complementary preclinical tools which provide compositional information on cortical bone components [16, 27, 55, 56]. Water, collagen and mineral -related spectral absorbance, can quantitively reflect the variation in bone composition.

Raman Spectroscopy

Raman spectroscopy is an inelastic light scattering technique that excites molecules through an incident laser photon in biological tissues [57-59]. A monochromatic incident radiation is illuminated onto a sample and this interaction causes light to scatter. The frequency of the scattered radiation is measured, and if it is the equal to the incident light it is known as Rayleigh scattering. Raman spectroscopy involves the measurement of a small of fraction of radiation that scatters differently from the initial beam of light, occurs as Stokes and Anti-stokes Raman scattering [59]. Stokes scattered light has a lower frequency than the incident light, and the interaction between the sample and the incident light causes the molecules within the sample to transition from a lower to a higher energy level. In contrast, anti-Stokes scattered light has a higher frequency than the incident light [58, 59]. Due to molecules transitioning to higher frequency it is to be noted that Anti-Stokes bands are comparatively not as intense as Stokes bands.

This inelastic mostly Stokes scattering causes changes in polarizability of a molecule leading to molecular vibrations of bonds at specific frequencies. A typical Raman spectrum ranges from 10-4000 cm^{-1} and consists of various vibrational modes (bending, stretching, wagging, rocking) that is represented as peaks with wavelength shift (x-axis) and intensity (y-axis) [57, 58]. Therefore, each type of bond gives rise to a particular molecular vibration at specific frequencies in a chemical group in a Raman spectrum. Raman spectrometers consist of several parts including a monochromatic laser source, typically in the visible and near infrared regions, optics (beam splitters, bandpass filters and mirrors) and CCDs, coherently working together to help generate a spectrum [58, 60]. There is little to no sample preparation to collect a Raman spectrum. Similarly, FT-IR is a technique that utilizes light in the infrared (IR) region of the electromagnetic spectrum. Depending on the frequency ranges, the IR region is divided into far-IR (FIR) (10-400 cm^{-1}), mid-IR (MIR) (400-4000 cm^{-1}) and near-IR(NIR) (4000-12,000 cm^{-1}) [61]. Molecules within a sample absorb infrared light at a frequency that is unique to their functional groups. This absorbed IR light causes molecular bonds to mainly bend or stretch leading to a signature spectrum. The differences between FT-IR and Raman methods is that in both cases the respective incident light strikes tissues, and molecules vibrate however, Raman scattering is sensitive to changes in bond polarizability, whereas FT-IR is sensitive to changes in dipole moments.

Even though molecular changes in tissues can be obtained through both modalities, Raman spectra tend to have lower signal to noise ratios, and auto fluorescence caused by light scattering, which introduce artifacts into the spectra [27, 57, 62]. Akkus and his group have evaluated changes in water content in bovine bone with Raman spectroscopy [16 , 63]. The data acquired in their studies does not represent spatial distribution of components throughout the entire bone tissue, but rather is an average of spectra from a few locations. Compared to MIR and NIR, Raman spectroscopy is not very well established for assessment of water content in tissues.

Infrared Spectroscopy

Most of the data in this thesis has been collected from the NIR spectral region. IR radiation is passed through a sample triggering a vibrational excitation and a change in the dipole moment of chemical bonds[64]. In an IR spectrum, the functional groups within a chemical structure produce unique absorption bands that are located at specific wavenumbers (frequencies) related to their bond length and mass [64, 65]. There are several modes of bond vibration such as bending, stretching, rocking and scissoring. The number of fundamental vibrations is determined by the molecular degrees of freedoms, for a molecule that is linear there are 3n-5 and for a non-linear molecule there are 3n-6, where n represents the number of atoms in the structure [65].

FT-IR Instrumentation

A typical FT-IR spectrometer consists of a source, a Michaelson interferometer and a detector [64, 66]. FT-IR spectrometers allow for fast acquisition of spectra from the entire frequency range of 400-12,000 cm^{-1}. As seen in Figure 5, the main component of a FT-IR spectrometer is the Michaelson interferometer. It consists of a beam splitter and two perpendicular mirrors where one is stationary and the other is movable [66].

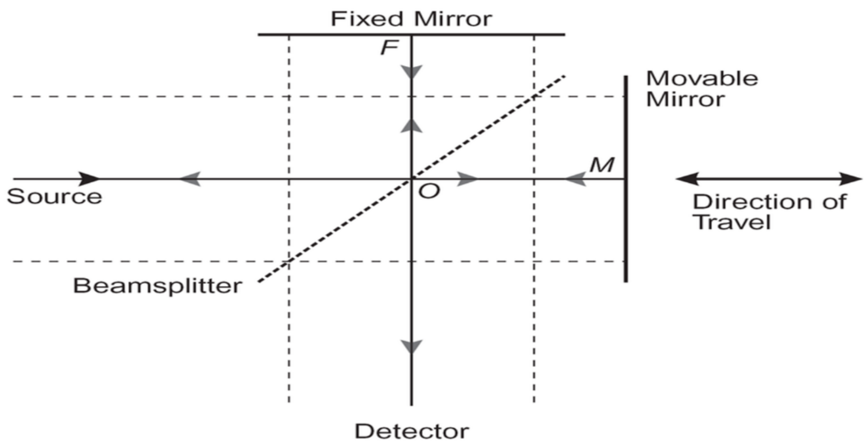

Figure 5: Schematic of a Michaelson interferometer [66].

A collimated IR beam hits the beam splitter causing half the length of light to be transmitted to the stationary mirror and the other half of light to be reflected onto the moveable mirror. The two beams of light recombine constructively or destructively at the beam splitter depending on the wavelength of light and optical path difference. This recombined light is directed onto the sample and transmitted or reflected to the detector as a digital signal known as an interferogram. The resultant spectrum is then generated by performing the Fourier transform of the interferogram [64, 66]. A typical spectrum consists of units in wavenumbers (cm^{-1}) and intensity in the x and y-axis, respectively. A background spectrum is collected prior to sample spectrum collection and ratioed to the sample spectrum to eliminate atmospheric and spectrometer interferences.

FT-IR coupled with a light microscope and an array detector, typically mercury cadmium telluride (MCT), can rapidly collect spatially distributed images that encode for relative amount, molecular nature and orientation of tissues in a short period of time[67]. This technology is known as FT-IRIS (Fourier transform infrared imaging spectroscopy), which refers to collection of spatially distributed images with a resolution as high as 6.25 microns in both the MIR and NIR spectral regions [67].

The two main modes of collecting data in IR spectrometers are transmittance and reflectance.[66] Transmittance is the simplest mode of data collection where the sample is placed between the IR radiation source and a detector, and some of the radiation is absorbed by the sample, and some transmitted. In reflectance, IR radiation is focused onto the surface of the sample where the light is either reflected, absorbed or scattered. Reflectance mode is further subdivided into specular and diffuse, a mirror- like reflection of light and scattering of light, or in all directions from the sample surface, respectively. In addition, transflectance is a mode where a thin sample is placed on a reflective slide, IR radiation passes through the thin sample in transmittance, reaches the reflective surface and is reflected back through the sample to the detector.

Attenuated total reflectance (ATR) sampling in FTIR is a popular method that allows for fast acquisition of spectral data with minimal sample preparation in the MIR region [68]. In this technique as seen in Figure 6, a beam of IR light at an angle is focused onto a crystal with a high refractive index, like diamond or Ge. This causes the IR light to reflect several times within the crystal creating an evanescent wave that interacts and penetrates a few microns into the sample surface, dependent on the specific frequency. This attenuated light then reaches the detector to and a spectrum is generated. An important aspect of ATR data collection is having good contact between the ATR crystal and the sample to ensure that the IR light is penetrating through the sample surface.

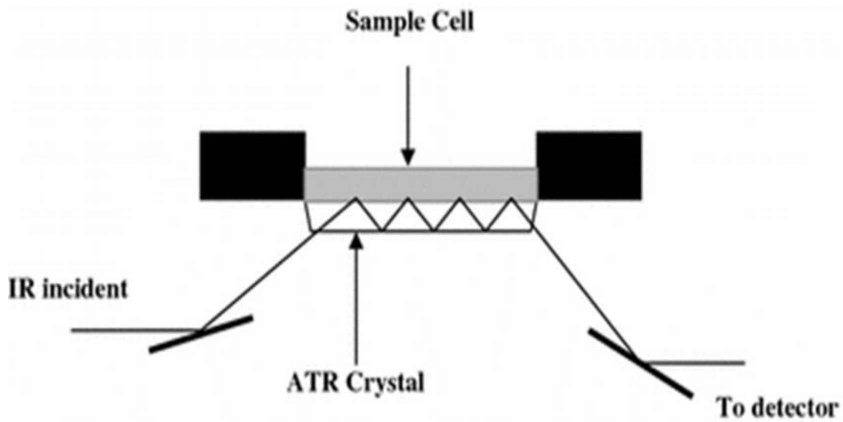

Figure 6: Schematic of ATR [69].

MIR radiation excites fundamental bending and stretching molecular bond vibrations from 400--4000 cm^{-1} [64]. A typical MIR spectrum of bone as seen in Figure 7 consists of a carbonate peak at ~ 850-890 cm^{-1}, a very broad phosphate peak around 900-1200 cm^{-1}, distinct protein peaks, amide I and II, a collagen peak at 1338 cm^{-1} , and two water absorbances at 1640 cm^{-1} and 3300 cm^{-1}[67]. The mineral absorbance at 900-1200 cm^{-1} is a result of bending and stretching of P-O bonds in phosphate, the amide I absorbance arises from the carbonyl stretching mode, the 1338 cm^{-1} peak originates from collagen side chain vibrations of CH_2 bending , and the water absorbance at 1640 cm^{-1} and 3300 cm^{-1} are from O-H bending and stretching respectively [67]. The MIR peaks that arise from the components of bone are very well established and can be used to aid in understanding the absorbances in another IR spectral region, such as the near infrared.

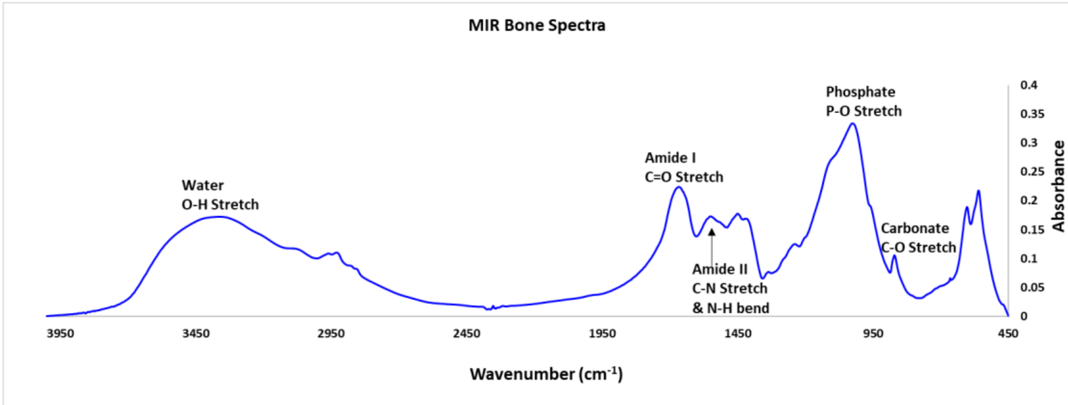

Figure 7: MIR spectrum of cortical bone.

The advantage of NIR over other infrared spectral ranges is its high depth of penetration of several millimeters - centimeters into samples [27]. A typical NIR spectrum consists of combination (4000-5300 cm^{-1}) and overtone (1st: 5300- 7100 cm^{-1}, 2nd: 7100- 9090 cm^{-1}) stretching and bending vibrations of O-H, N-H, S-H, and C-H bonds, which have their fundamental vibrations in the MIR region [70]. A characteristic NIR spectrum from human cortical bone can be seen in Figure 8. Some collagen absorbances in the MIR arise from CH_2 bending at 1338 cm^{-1} and from N-H stretching at 3200 cm^{-1}, and the counterpart of these two absorbances are located in the NIR in the combination region and first overtone region at 4608 cm^{-1} and 6688 cm^{-1} respectively [27, 67]. Cortical bone water absorbances in the MIR region originate from O-H bending (1640 cm^{-1}) and stretching (3300 cm^{-1}) mode, and in the NIR region, are located in the combination and in the first over tone region at ~5184 cm^{-1} and ~7000 cm^{-1} in NIR respectively. One drawback in using NIR is the low absorptivity of mineral vibrations in the NIR region. Even though a substantial phosphate absorbance from hydroxyapatite, the primary component of bone, is detected centered at ~1030 cm^{-1} in the MIR region, it's counterpart in the NIR region doesn't exist.[68] Recently it has been reported that phosphate associated with a hydroxyl vibration (P-OH) in mineral has been detected at ~7000 cm^{-1}, yet there needs to be further confirmation of this peak [27, 71].

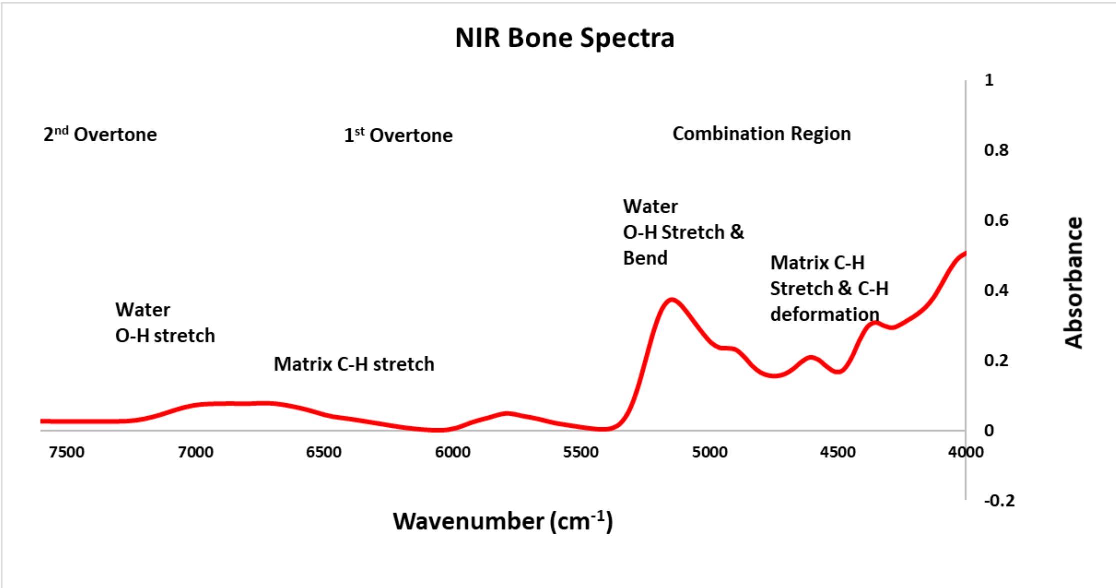

Figure 8: NIR spectrum of cortical bone.

NIR spectral pre-processing techniques

Scatter corrections

Raw NIR spectra is affected by additive and multiplicative scattering, which causes spectra to be modified or scaled by a certain factor, and tend to have baseline displacements in the y-axis due to path length differences in samples [72]. Multiplicative scatter correction (MSC) helps to reduce scatter by regressing the measured spectrum to an ideal spectrum. This spectrum is typically an average spectrum from the measured data set. The additive and multiplicative scatter is corrected in the spectra by applying the intercept and slope values derived from the average spectrum [73]. An MSC correction is not wavelength dependent, which could improve the signal correction. An extended multiplicative scatter correction (EMSC) allows for the discrimination of the physical light scattering from the chemical absorbances based on wavelength-dependent signal correction [74].

Second Derivative

Application of derivatives is a frequently used method for preprocessing spectra because it enhances resolution of underlying absorbances that cannot be observed in raw spectra, and also reduces non-linear baselines in the data [75]. The first derivative pertains to the rate of change y (absorbance) with respect to x (wavenumber). Second derivative spectra are twice differentiated from raw spectra. These second derivative spectra can be used to acquire quantitative data regarding the sample, as the constant and linear components are not affected during differentiation. Therefore, the peak height in the second derivative is directly correlated to amplitude of the absorbance in the raw spectra [75]. Typically, smoothing along with differentiation are applied to raw spectra to enhance the signal to noise ratio. One such method is the Savitzky-Golay filter which uses a fitted polynomial to smooth and transform the raw to derivative spectra [73]. The number of smoothing points must be optimized based on the signal to noise level in the spectra. For example, too many points will reduce the noise, but can also remove useful information pertaining to the sample.

Univariate and multivariate analyses

Two main methods to quantify NIR data are by application of univariate and multivariate analyses. Univariate analysis is the simplest and the fastest method to analyze spectral data. In MIR data, typically absorbance integrated values are calculated and ratioed to other integrated absorbance values to understand the relative amounts of components. For example, to understand age related changes in bone mineral content, the ratio of area under the mineral phosphate (1030 cm^{-1}) and matrix (amide I) (1650 cm^{-1}) absorbances can be analyzed [67]. Similarly, the area under the amide I absorbance is used to estimate the total amount of protein [76]. To quantify spectral data, according to Beer's law equation (1) the amount of IR radiation that is absorbed by the sample (A) is correlated to concentration [64, 66].

$$Equation\ (1): A = \varepsilon\ l\ c$$

In equation 1, A is the absorbance, ε is molar absorptivity constant which depends on the wavelength (or frequency), l is the path length and c is concentration.

Therefore, the integrated values for specific absorbances correlate to the amount of a component. Differentiation of equation (1) is a linear method, therefore, the second derivative peak height still correlates to the peak height in the original signal [75] In NIR, absorbances tend to be broad and O-H bonding of water overwhelms the spectra; therefore, second derivative Savitzky-Golay filters are frequently applied to resolve the underlying peaks [27]. This is an effective method to investigate single peak variations.

Multivariate analysis such as principal component analysis (PCA) and partial least squares (PLS) are two common statistical methods used to analyze spectral data. PCA is a dimensionality reduction method that attempts to simplify complex datasets by finding patterns between samples and variables. PCA is an exploratory analysis of data. In PCA the variance in the original data set is explained in terms of a smaller number of independent linear combinations known as principal components (PC). PLS is an extension of PCA that attempts to use PC's and linearly correlates to Y variables. PLS quantitively explains the variance in the data through factors and helps to find a linear correlation between X and Y variables. In spectral data, X (predictors) are each spectral frequency from 4000-12000 cm^{-1} and a Y response variable is a measurement of tissue's physical property such as gravimetrically derived water content [77]. PLS calibration models are first validated by cross validation techniques and then the developed model utilized to independently predict response variables with only spectral input. The leave one out cross validation technique uses each individual spectrum to either calibrate or validate the data structure. The strength of the calibrated and predicted models is based on low root mean square error (RMSE) and high R^2 values. The two main outputs in PLS models are scores and loading plots. A scores plot visually explains the properties of samples by separating the data based on similarities and differences within the tissues. The loadings plot explains the variance in terms of factors that causes the separation in the data structure of the scores plot. Most of the variance in data is explained within the first few factors of the loadings plot.

1.7 FT-IR Analysis of Cortical Bone

FT-IR in the NIR region also known as near infrared spectroscopic imaging (NIRSI), has been applied to study water content for musculoskeletal tissues such as cartilage and bone [27, 78]. The sensitivity of NIR spectra to water and the ability to collect chemical absorbance maps that reflect spatial distribution of components throughout a sample in a short amount of time has motivated further research to use

NIRSI to investigate bone quality. NIRSI has shown to be an effective preclinical tool for bone quality assessment, since there is little to no sample preparation to acquire information on the spatial distribution of components in bone tissues [27]. NIRSI can help to provide molecular insight into collagen and mineral as well as loosely or tightly bound water. NIR has been used to identify some primary components of cortical bone, [27] however understanding how the gradual dehydration of aging tissues impacts its organic and inorganic matrix has yet to be assessed. Therefore, NIR is an ideal non-destructive, non-invasive tool to evaluate cortical bone in-vitro for bone quality. NIR with univariate and multivariate analysis can be used for cortical bone quality, in conjuncture with univariate and multivariate analysis.

1.8 Evaluation of Cortical Bone Water Content in Animal Models

Information regarding age-dependent changes in bone stem from evaluating small and large animal models for preclinical bone quality assessment. Bulk tissues from mice, rats, bovines and human cadavers have been excised for mechanical testing and evaluation of bone architecture and composition Several studies have correlated rodent, bovine and human cortical bone porosity from micro-CT to water content in tissues [79-83]. Increase in bone porosity is caused by the expansion of pores which displace and decrease loosely bound water causing a decrease in overall bone strength [84]. In micro-CT the 3D visualization of skeletal tissue architecture of pores and microdamage within the structure has aided in studying bone fracture propagation. Additionally, *in vitro* studies help to characterize bone mechanical properties. For example, dehydration of bones produces similar stress on collagen fibrils recapitulating what is seen in aging tissues. It has been determined with age the accumulation of microdamage the mechanical competence changes in bone tissues. Nyman and his group performed 3-point bend tests to evaluate the toughness and stiffness of dehydrated bones [85]. They found that collagen fibrils decrease in diameter and contract longitudinally, reducing the sites for water molecules to bind and therefore the overall toughness of bone decreases. A study by Yan et al., showed that in bovine femurs there was a 45% decrease in bone tissue toughness between hydrated (5.5 $MPa{\cdot}m^{1/2}$) and dehydrated (3.8 $MPa{\cdot}m^{1/2}$) samples [86]. Several studies indicate that changes in the spacing between each collagen fibril in aging bone directly impacts the mechanical properties causing bone to become more brittle and fragile [87-89]. A similar pattern of reduction in mechanical competence can be seen with aging male tissues, summarized in Table (1) [90].

Table 1: Mechanical properties of aging male tissues [90].

Age Groups no. of Samples	≤30 (4)	31-50 (5)	51-70 (6)	≥70 (4)
Tensile strength MPa	39.23 ± 2.28	35.95 ± 3.86	26.03 ± 1.95	19.65 ± 1.48
Compressive strength MPa	143. 35 ± 2.35	131.21 ± 6.63	107.41 ± 8.07	96.35 ± 0.84
Young's modulus MPa	197.01 ± 20.37	234.36 ± 17.88	312.25 ± 83.62	964.43 ± 195.78

Preclinical studies have allowed for a comprehensive assessment of cortical bone at every scale. Structural information can be studied through micro-CT, compositional components are evaluated by vibrational spectroscopy and the mechanical competence of bone is assessed by various tests including compression, tensile, 3 or 4-point bend tests.

A continued interest persists to understand the changes that occurs in aging skeletal tissues. Previous studies have helped to clarify some questions but there continues to be discrepancies in evaluating bone quality. For example, preclinical studies have helped to shed light on the limitations of BMD and other markers such bone water need to be further validated as reliable indicators for bone fragility assessment. Development of the NIRSI technique to predict water content will help to detect and monitor diseases states to provide a better understanding of bone pathology.

CHAPTER 2: HYPOTHESIS AND SPECIFIC AIMS

There is growing evidence that age related changes in bone water associated with collagen and/or mineral has a direct impact on the structural integrity of bone. This Ph.D. thesis focuses on developing a NIRS method for evaluation of specific water compartments associated with collagen and mineral in cortical bone.

2.1 Hypothesis

NIR-determined water associated with collagen and/or mineral in cortical bone can be used as a biomarker for bone quality assessment in future preclinical studies.

2.2 Specific Aims

1. Design and build an environmentally controlled chamber for NIR bone tissue imaging.

The outcome of this Aim will be a chamber that can main a constant humidity for durations long enough to collect data from small or large bone samples with minimal fluctuations in NIR-determined water absorbances.

2. Identification of NIR absorbances of water loosely and tightly bound to bone collagen and mineral, and confirmation of correlation of NIR-determined water absorbances with gravimetric water content.

2A. NIR prediction of overall water content (creation of calibration curve based on NIR spectra).

2B: Determination of loosely and tightly bound water to collagen and mineral.

2C**:** Quantification of NIR mineral-associated absorbances based on P-OH bonds.

The overall outcome of this Aim will enable prediction of total water content in bone based on NIR spectral absorbances. Additionally, this aim will also help to elucidate NIR loosely and tightly bound water compartments associated with collagen and mineral, as well as identify NIR mineral absorbances.

3. Correlate NIRSI-determined water content in human cortical bone to structural properties (micro-computed tomography (micro-CT) analysis).

The outcome of this Aim is to correlate the identified NIR water compartments associated with collagen and mineral in aim 2 to structural properties in aging cortical bone samples.

These Aims will be addressed in Chapter 3 and 4 of this thesis. Together, these studies support a great need for increased understanding of the role of water content, distribution and binding in bone quality assessment.

CHAPTER 3: ENVIRONMENTALLY-CONTROLLED NEAR INFRARED SPECTROSCOPIC IMAGING CHAMBER

Studies in Chapter 3 have been resubmitted after revisions to Scientific Reports. In this study an environmentally- controlled imaging chamber was designed for NIRSI. The chamber was validated in high and low relative humidity to understand the effects of environmental changes during imaging in cortical bone water content. This chamber was used to collect NIRSI spectral data from human cadaveric cortical bone samples and a calibration curve was generated to predict gravimetric water content. The results discussed from this Chapter pertain to Aims 1 and 2A.

3.1 Abstract

We have designed an environmentally-controlled chamber for near infrared spectroscopic imaging (NIRSI) to monitor changes in cortical bone water content, an emerging biomarker related to bone quality assessment. The chamber is required to ensure repeatable spectroscopic measurements of tissues without the influence of atmospheric moisture. A calibration curve to predict gravimetric water content from human cadaveric cortical bone was created using NIRSI data obtained at six different lyophilization time points. Partial least squares (PLS) models successfully predicted bone water content that ranged from 0-10% ($R= 0.96$, $p<0.05$, root mean square error of prediction (RMSEP) =7.39%), as well as in the physiologic range of 4-10% of wet tissue weight ($R=0.87$, $p<0.05$, RMSEP = 14.5%). Similar results were obtained with univariate and bivariate regression models for prediction of water in the 0-10% range. Further, we identified two new NIR bone absorbances, at 6560 cm^{-1} and 6688 cm^{-1}, associated with

water and collagen respectively. Such data will be useful in pre-clinical studies that investigate changes in bone quality with disease, aging and with therapeutic use.

3.2 Background

Water is an important contributor to bone quality, and makes up ~approximately 10% of cortical bone wet weight [91]. Increased fracture risk and bone fragility have been associated with a decrease in the overall skeletal tissue water content [21, 22, 25]. However, specific regions associated with water changes have not been fully elucidated. In cortical bone, water generally can be found as tightly and loosely (surface) bound to either collagen and mineral, and within the pore network. In collagen, the helical structure is stabilized via intramolecular and intermolecular hydrogen bonding of water molecules [17]. In mineral, water molecules are in part tightly bound to carbonated crystals in the apatite core [13]. Water is also loosely bound to the amino acid side chains in collagen, as well as to the surface ions in mineral crystals. Additionally, surface water is also found between the collagen and mineral interphase [16, 94].

Cortical bone water content has been evaluated through several destructive and nondestructive techniques [16, 25, 58, 87, 95, 96]. Gravimetric analysis is considered a gold standard method for evaluation of water content in biological tissues [95]. Nevertheless, since this method is destructive and time consuming, it has motivated development of nondestructive techniques that can be applied for assessment of water related to bone quality. One such method is NIRSI, a technique based on radiation in the near infrared region (NIR) of the electromagnetic spectrum, 4000 – 13000 cm^{-1}. The sensitivity of NIR to water has been widely studied as a quality parameter in the food science, agricultural and pharmaceutical industries [98 –103]. NIR spectra are comprised of overtones and combination absorbance bands from molecular vibrations of C-H, O-H, S-H and N-H bonds [27, 79]. However, a typical spectrum in the NIR consists of overlapping bands dominated by water O-H absorbances, which can make it challenging to interpret spectral absorbances from non-aqueous components. In contrast, one primary advantage of NIR is that it penetrates several millimeters into a sample, which permits a full-depth chemical analysis of biological tissues and materials [102].

NIRSI has been utilized to study water content in musculoskeletal tissues such as cartilage and bone. Padalkar et al.[103] evaluated water content in articular cartilage by gravimetric and NIR techniques, and NIRSI helped to differentiate between free (6890 cm^{-1}) and bound (5200 cm^{-1}) water in cartilage. More recently, Rajapakse et al. [52] non-destructively evaluated compositional changes in aging cadaveric cortical bone tissues by NIRSI for skeletal quality assessment, and correlated matrix (4608 cm^{-1}) and water absorbances to MRI-derived water content in the same tissues. Together, both studies showed that NIRSI is a sensitive method for evaluation of changes in tissue water content, and correlation to other conventional techniques.

Other nondestructive techniques that have been used to evaluate cortical bone water content are Raman spectroscopy [16], [56] and magnetic resonance imaging (MRI). Unal et al. [91] conducted dehydration studies in bovine cortical bone samples to determine Raman spectral water absorbances that can be used as biomarkers for bone quality assessment. That study labeled Raman spectral absorbances for water compartments in cortical bone as bulk water, collagen-bound water, mineral-bound water and water associated with mineral and collagen [104]. Even though individual peak intensities at specific time points of dehydration where useful for assessment of changes in water, the instrumentation used for the analyses was custom built, and not widely available. Many common Raman spectrometers produce spectra that can have very low signal to noise ratios, and fluorescence interference can be a problem during data analysis [105]. MRI imaging of water has the advantage of being applicable to clinical studies, and several studies have investigated changes in water content in tissues for bone quality assessment [52, 83, 106]. Drawbacks of MRI analyses are that only collagen-bound water and pore water can be detected currently, and mineral-bound water signatures are not available. Further, in clinical MRI studies, the best resolution is generally on the order of a few hundred microns. In contrast, NIRSI will allow for data acquisition at a pixel resolution as high as 6.25 microns [27,107].

One major challenge in evaluation of water content using spectroscopic techniques is the constant fluctuations in hydration and dehydration of tissues during data collection. Recent studies that have evaluated cortical bone water content using NIRSI and Raman spectroscopy have acquired data in atmospheric conditions [27, 91]. Depending on the atmospheric humidity, and the time required for data collection, tissues may undergo a reoccurring change in their water content which may be reflected over time in their spectra by a potential increase or decrease at the frequencies of water absorbances. Consequently, the repeatability of studies may be challenging, in particular during water calibration studies [108].

Motivated by the challenges with water vapor fluctuations, and the need to definitively identify NIR absorbances from mineral and collagen components in bone, we designed and implemented an environmentally-controlled chamber to optimize the collection of NIR spectral imaging data from biological tissues. This is a partially sealed chamber that allows for air flow at a constant humidity level. Thus, the water loss and gain during data collection is reduced and changes in atmospheric factors, such as water absorbances, are minimized. Here, we describe the chamber, and subsequent experimental NIRSI data obtained from serially dehydrated bones with a range of water content. Utilizing multivariate analysis, we established a calibration curve from which gravimetric water content can be predicted from NIR spectral data obtained from human cortical bone in the chamber. In addition, serial dehydration of bone enabled identification of absorbances attributed to non-aqueous components of bone. These studies will provide a firm foundation for NIRSI evaluation of water content in harvested bone, and for pre-clinical studies of bone quality.

3.3 Methods

Tissues

The environmental chambers were validated using NIRSI data obtained from tibiae from young bovine bone (Research 87, Bolyston MA). The calibration curve data were obtained from cadaver human tibiae harvested from 19 donors with no evidence of skeletal disease (13 male and 7 females, exempt from IRB protocols) (NDRI, Philadelphia, PA). Bones were stored frozen at −20 °C and thawed for gravimetric and NIRSI data acquisition.

Bone Sample Preparation

Bovine and human cadaveric cortical bone samples were prepared for data collection as follows: Tissues were cut cross-sectionally to a uniform thickness of 500 μm from the regions of maximum cortical bone thickness (~10% distance proximal to distal endplate) with a diamond wafering saw (Buehler Isomet 1000, Lake Bluff, IL). The samples were ultrasonicated (60 khz FS60D Fisher Scientific) in 1% tergazyme solution for 2 hours at 38°C to remove bone marrow. Marrow-free specimens were stored in phosphate buffered saline-protease inhibitor (PBS-PI) (PBS 1×, pH 7.4, Invitrogen, Carlsbad, CA) with, protease inhibitor (Sigma-Aldrich, St. Louis, MO)), at -20°C until data collection.

Environmental Chamber Design Small chamber

To evaluate bone samples under constant humidity, an initial chamber was constructed from a glass microscope slide base, laser cut cast acrylic walls and lid, and a glass cover slip viewing window. Plastic inlets and outlets were installed on the top of the chamber to facilitate airflow. An Arduino driven Bosch BME-280 humidity sensor (Stuttgart, Germany) logged RH data inside the chamber. Humidified air flow was generated from a 4psi pump aerating a 50mL conical vial partly filled with room temperature water and fed into the imaging chamber through plastic tubing. This setup maintained a 72 ± 2% RH environment inside the chamber for over two hours. A desiccated environment was achieved by feeding the chamber with compressed air at 4 psi.

Large chamber

To collect NIRSI data from larger, clinically-relevant human bone samples, a larger imaging chamber was constructed from cast acrylic and two 76.2x76.2x0.5 mm Corning® Gorilla® Glass imaging windows (Corning, NY). Like the previous chamber model, RH data was logged from an Arduino-driven Bosch BME-280 humidity sensor. When compressed air at 4 psi entered the large imaging chamber, the internal RH quickly dropped to 0% and that level was maintained for the experiment duration. This insured no environmental moisture was absorbed by the bone samples.

Environmental Chamber Validation

NIRSI data were collected from a specified 400 x 400-micron region from bovine bone samples inside the environmental chamber using a Perkin Elmer Spotlight 400 imaging system equipped with a mercury cadmium telluride (MCT) detector (Shelton, CT) every 15 minutes over the course of one hour before, and again after, a 24-hour lyophilization in a lyophilizer (Martin Christ-Alpha 1-2) . Chambers were validated by the assessment of changes in the 5184 cm^{-1} absorbance within a 60-minute timespan. The 24-hour lyophilization period was chosen after confirmation in pilot studies that no additional water was lost after this period of lyophilization. The samples before and after lyophilization were termed wet and dry bone, respectively.

NIRSI data collection for chamber validation

The spectral data were collected at 50 µm spatial resolution with 32 coadded scans at 64 cm^{-1} spectral resolution in the frequency range from 4000–7800 cm^{-1}. The experimental setup depicted in Fig. 9 allowed the small chamber to maintain RHs of less than 3% and at 0%. The small chamber was additionally tested at high RH of ~70%.

NIRSI data processing and analysis for chamber validation

The spectral data collected at low and high RH were quantified for bone water content by processing raw data to derive the second derivative (Savitzky Golay, 2^{nd} order polynomial and 7 points of smoothing, inverted to make peaks positive) average pixel intensity, and assessment of an established NIR water absorbance of 5184 cm^{-1} in ISys 5.0 software (Malvern Instruments, UK). It was previously shown that the average pixel intensity measurement at 5184 cm^{-1} generally correlates to the water present in the sample [27].

Statistical Analysis

Mean values ± standard deviations are reported for quantitative data. Analysis of Variance (ANOVA) with Tukey post hoc test was used to evaluate the differences in mean values for experimental data, with $p<0.05$ considered statistically significant**.**

Water Calibration Curve Experimental Setup (Fig. 9)

The optimal conditions determined in the chamber calibration process were applied here to generate the water calibration curve. The large chamber was used to collect NIRSI data at 0% RH for the water calibration curve. The experiment consisted of sequential dehydration of human cortical bone tissues through lyophilization and collection of NIRSI data at specific timepoints. Gravimetric and NIRSI data were collected from two different locations in each specimen at the following 7 timepoints:

lyophilization for 5 minutes to uniformly remove excess surface water, then subsequent serial lyophilization for 15, 25, and 120 minutes, and 24 and 48 hours.

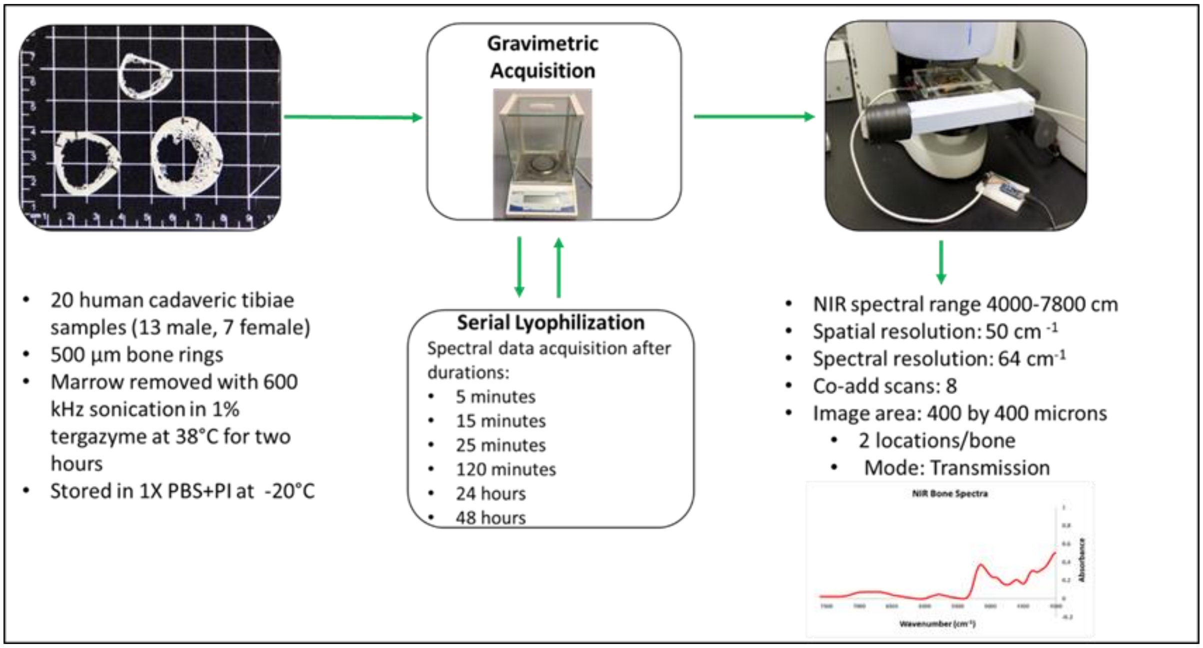

Figure 9: Schematic of the experimental setup for data collection from human cadaveric tissue samples used in creation of the water calibration curve. (© 2018 PerkinElmer, Inc. All rights reserved. Printed with permission).

Gravimetric data collection and analysis for calibration curve

Initially, human cortical bone samples were thawed and dabbed dry with a Kimwipe to remove residual PBS-PI solution. Samples were weighed after every lyophilization treatment on a SI 215D Denver Instruments (Bohemia, NY) Precision Balance for gravimetric analysis. To determine the percent of water content within the tissues the wet weights were calculated as follows:

Equation 1:

$$\frac{Wet\ weight_{(W)} - dry\ weight_{(D)}}{Wet\ weigh\ t_{(D)}} * 100$$

.

- Wet weight $_{(w)}$ = sample weight at every dehydration timepoint.
- Dry weight $_{(D)}$ = sample weight with 48 hours of lyophilization.

NIRSI data collection for calibration curve

NIR spectral data was collected from two different 400 x 400-micron marked areas for each sample using a Perkin Elmer Spotlight 400 imaging spectrometer. The NIRSI data was collected in the large environmentally controlled chamber with a RH of <3% at a frequency range 4000–7800 cm^{-1} at 64 cm^{-1} spectral resolution and 50 μm spatial resolution with 32 coadded scans, and an approximate imaging time of 2 minutes at each location.

NIRSI data processing and analysis for calibration curve

NIR spectral image were analyzed using ISys 5.0 and UnscramblerX 10.4 (Camo, Norway) software. One average spectrum was calculated for each spectral image. For 19 human cadaveric samples, a total of 302 averaged spectra were used for data processing. Second derivative processing (Savitzky Golay, 2nd order polynomial and 7 points of smoothing) was applied to normalize and resolve broad peaks in NIR spectra. The optimum number of 7 smoothing points was chosen after careful analysis of spectra, since the goal was to minimize noise while maximizing peak resolution in the dataset (Fig. 10). NIR second derivative absorbances (inverted, to make peaks positive to facilitate understanding data) were evaluated from water components at 5184 cm^{-1}, 6560 cm^{-1} and 7008 cm^{-1} and from matrix at 4608 cm^{-1} and 6688 cm^{-1} [27]. Approximately 82 data points were removed from the analysis either due to spectral artifacts caused by residual fat in tissues or to poor quality spectra based on low signal to noise. Therefore, 220 spectra were utilized in total for both univariate and multivariate analysis.

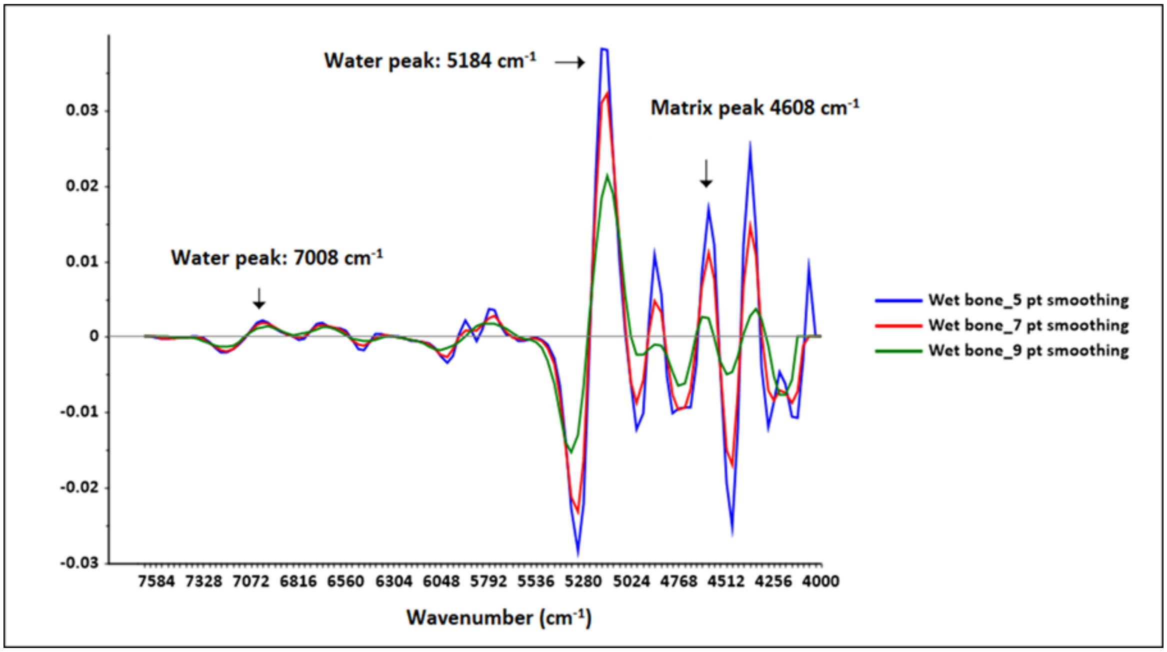

Figure 10: Inverted second derivative spectra of wet bone with varying smoothing points. Seven smoothing points was the optimal number since it had the best signal to noise ratio.

Univariate Analysis

Univariate analysis: Inverted second derivative spectra at 5184 and 7008 cm^{-1} water absorbances were correlated to gravimetrically-derived water content. The correlation R, p-values and root mean square error (RMSE) of cross validation are reported in below in table 2.

MLR is a statistical technique that helps to predict outcome variables based on one or more explanatory variables. MLR helps to model the linear relationship between the explanatory and outcome variables. In this study, the outcome variable is the gravimetric water content and the explanatory variables are the individual frequencies of water (5184 cm^{-1} and 7008 cm^{-1}) and matrix (4608 cm^{-1} and 6688 cm^{-1}). The strength of the regression is determined by high R and low RMSE values.

Multivariate Partial least squares analysis

Partial least squares (PLS) analysis is a statistical method used to find linear relationships between predictors and determinant variables[109]. The main advantage of using PLS in creating a linear regression is the ability to analyze multiple variables at a single time. This is very useful for analysis of NIR spectra as the spectra are typically composed of overlapping absorbance bands. PLS models were developed to predict percent water content with X determinants as the spectral data and Y predictors as the gravimetrically-determined percent wet weight. Spectra were randomly chosen (N =147) to build the model using a leave one out cross validation technique and the remaining 73 spectra were used for independent prediction. This process was repeated 3 times with spectra randomly chosen each time for model building and independent prediction. The strength of the models generated, and the independent predictions were determined based on a high R^2 and low root mean square error (RMSECV) values. The two main outputs in PLS models are the scores and loading plots. The scores plot visually explains the properties of samples by separating the data based on similarities and differences within the spectra. The loadings (or factors) plot explains the variance by examination of specific frequencies that cause the separation in the data structure of the scores plot. Most of the variance in data is explained by the first few factors.

3.4 Results

The results described below are based on the following approach where we assessed the optimal sampling method using environmental chambers. Initially, a small chamber was designed to evaluate NIR data collection from wet (hydrated) and dry bone samples in low and high relative humidity (RH), with the goal of determining which environment was most stable for data collection. Since the imaging area in the small chamber was limited by the size of the cover slip (Fig. 11), a large chamber was subsequently designed and validated for data collection from hydrated and dry clinical size bone samples (described following the small chamber results) (Fig. 12).

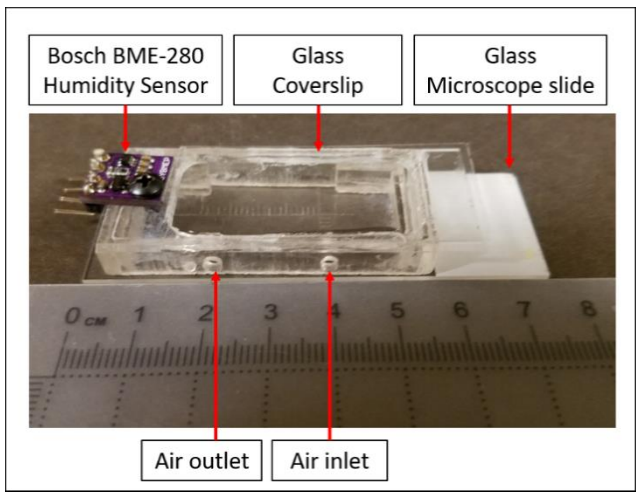

Figure 11: Small environmental chamber with input and output for airflow tubing, and humidity sensor.

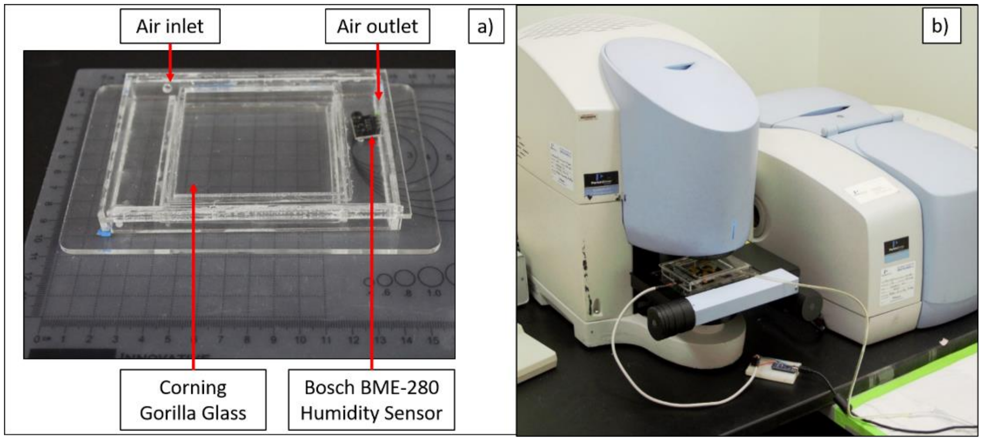

Figure 12: a) Large environmental chamber with input and output for airflow tubing, and humidity sensor. b) Data collection setup with chamber positioned on the Perkin-Elmer Spotlight 400 imaging spectrometer. (© 2018 PerkinElmer, Inc. All rights reserved. Printed with permission).

Optimization of Spectral Data Collection in an Environmentally-Controlled Chamber

The small chamber (Fig. 13a) continuously maintained either high or low RH for 60 minutes during NIRSI data collection (Fig. 13a & 13b). Collection of spectral imaging data from dry bone in a humidified environment resulted in absorption of moisture and a higher water content after 15 minutes of data collection (Fig. 13c). However, spectral acquisition from hydrated bone in a humidified environment resulted in minimal water absorption, likely due to those samples already being saturated (Fig. 13c).

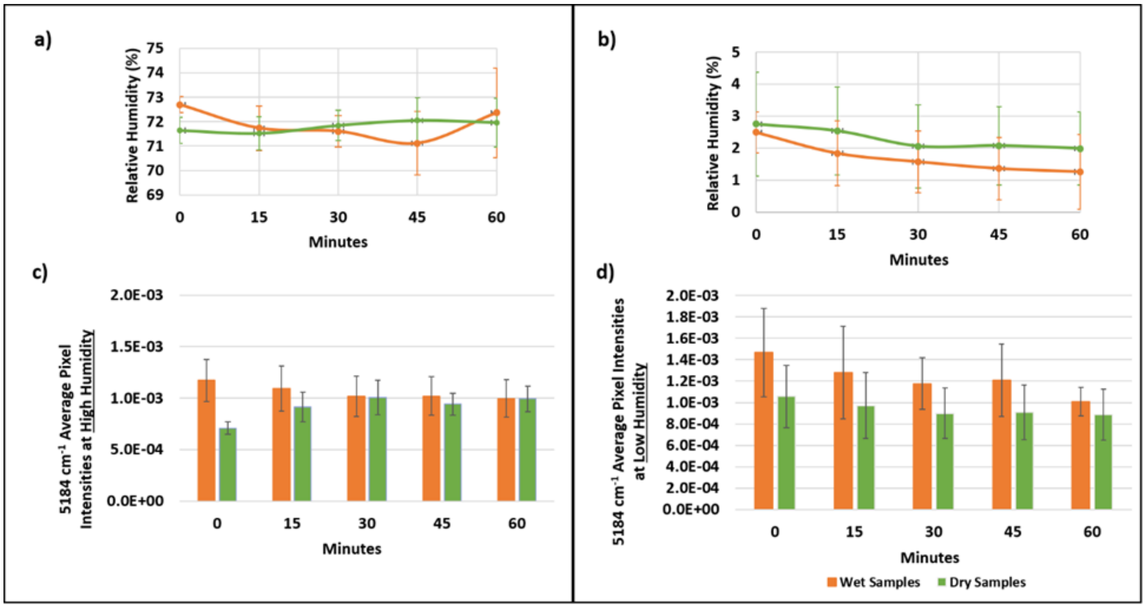

Figure 13: RH inside the imaging chamber during one hour of spectral data collection from wet and dry bone samples in high a) and low b) RH conditions. Average pixel intensity at 5184 cm^{-1} (inverted second derivative intensity of NIRSI water absorbance) inside the imaging chamber during one hour of spectral data collection from wet and dry bone samples in high c) and low d) humidity.

Conversely, in a low RH environment, neither hydrated or dry bone absorbed or lost a significant amount of water, and the water absorbance from the bone samples remained stable (Fig. 13d). Accordingly, low RH was determined the optimal condition for creation of the calibration curve from serially dehydrated bone samples, and the large chamber was only validated with low RH.

The validation of the large chamber was performed by periodic NIRSI data collection from marked areas of bone samples, combined with evaluation of changes in a well-defined NIR bone water absorbance at 5184 cm^{-1}. Once the data collection parameters were optimized, a NIRSI water calibration curve from cadaveric human bone samples of uniform thickness was developed using multivariate spectroscopic methods.

Further, NIR absorbances from non-aqueous components of bone were elucidated by analysis of dehydrated bone tissues.

The large chamber successfully maintained 0% relative RH for 60 minutes of data collection (data not shown). With NIRSI data collection from fully hydrated bone samples, an initial drop in intensity of the 5184 cm^{-1} water absorbance from 0 minutes to 15 minutes was observed, believed to be attributable to remnants of PBS evaporating from the surface of the bone (Fig. 14).

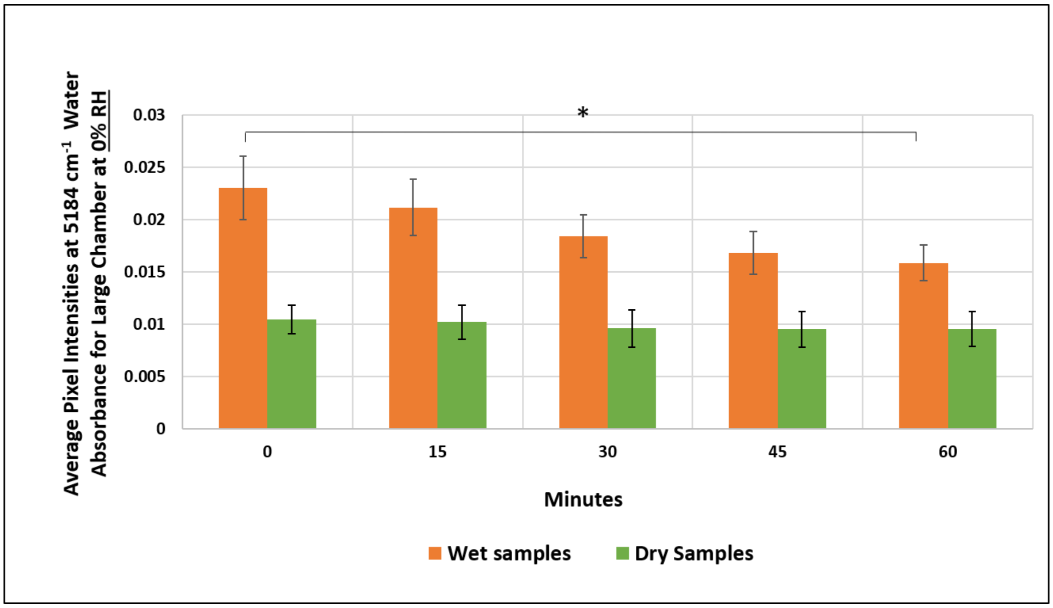

Figure 14: Average NIRSI pixel intensities at 5184 cm^{-1} (water content) of wet and lyophilized bone samples under 0% RH in the large chamber. Wet samples gradually lose water content over an hour, while dry samples maintain their water content. (*) Average pixel intensities at 5184 cm^{-1} for wet sample group at 0 and 60 minutes were statistically significant at $p < 0.05$.

The water content in hydrated bone incrementally decreased during 60 minutes of NIRSI imaging in low RH resulting in ~ 31 % water loss in bone overall (Fig. 14), with a statistically significant reduction in water content between the 0- and 60-minutes time points. However, for the dry bone samples, the average pixel intensity at 5184 cm^{-1} did not significantly change with time, and the chamber was able to maintain low constant RH for 60 minutes of imaging (Fig. 14). Based on these results, it was determined that calibration curve data collection, which would span collection of data from both hydrated and dry samples, could occur in low constant RH. However, data collection should start after a short drying period to minimize changes from bulk surface water loss and should not exceed 5 minutes. This would ensure that no significant changes in water content of the more hydrated samples would occur.

Identification of Absorbances from Non-Aqueous Components of Bone from Dehydration Studies

Raw (Fig. 15a) and second derivative spectra (Fig. 15b) obtained from serially-dehydrated samples were used for evaluation of changes in NIR bone water peak intensities at 5184 cm^{-1}, 6560 cm^{-1} and 7008 cm^{1}, and to elucidate NIR absorbances related to non-aqueous cortical bone components. The two main NIR bone matrix (collagen) absorbances were observed at 4608 cm^{-1}, a combination peak from C-H stretches and at C-H deformation, and at 6688 cm^{-1}, a 1st overtone absorbance from N-H stretching from amino acid side chains of collagen. Mineral-associated absorbances in cortical bone still need to be further validated, but based on a recent study, a potential P-OH vibration in the NIR range can be observed at approximately at 7000 cm^{1}[71].

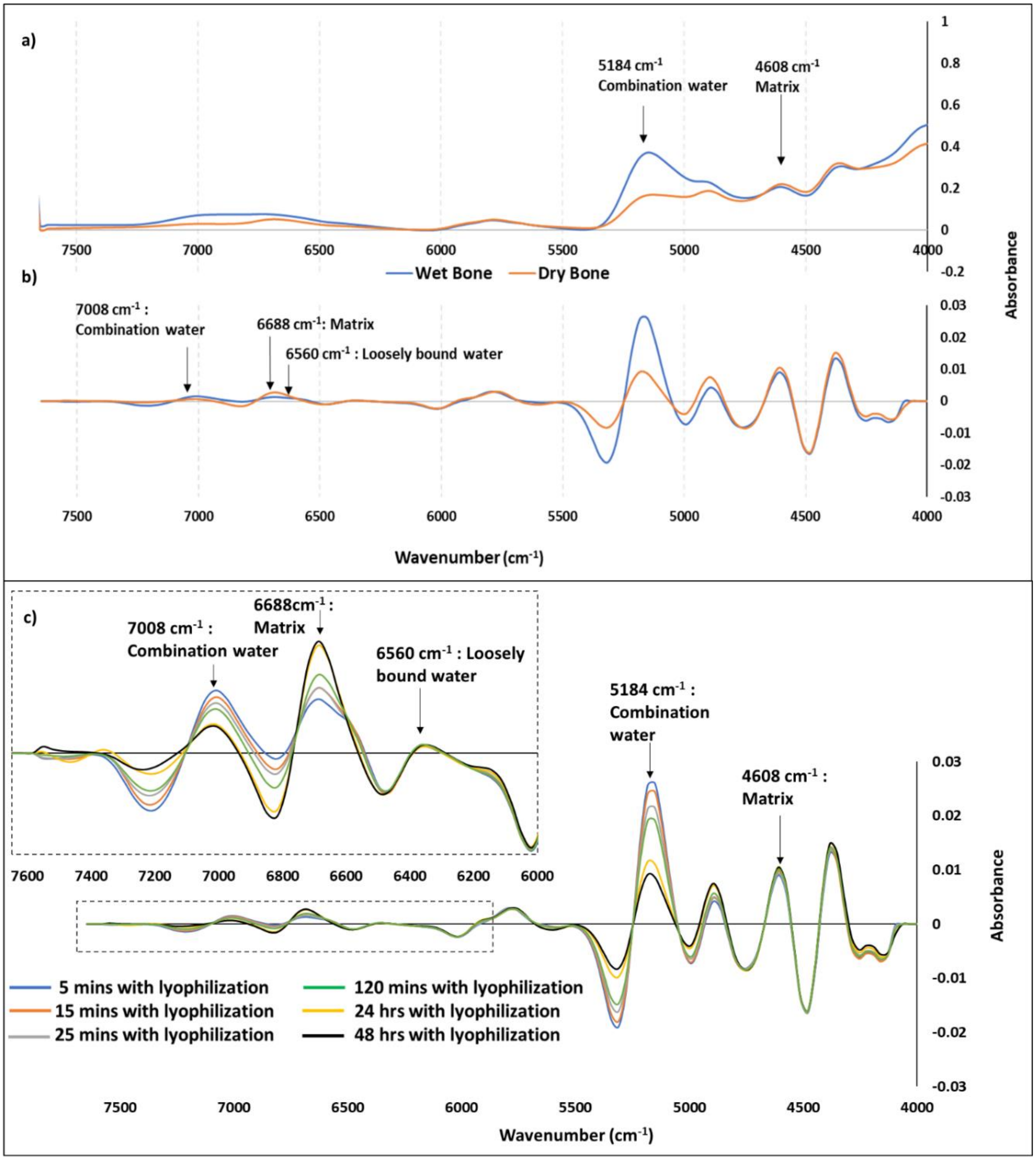

Figure 15: a) Raw NIR spectra of wet (hydrated) and dry bone. b) NIR second derivative of wet (hydrated) and dry bone. The water and matrix peaks are more resolved in the second derivative spectra compared to raw spectra. A reduction in the 5184 cm^{-1}water peak can be seen in both raw and second derivative spectra of dry bone. c) Second derivative NIR spectra of serially dehydrated bone. The absorbance of the water peaks (5184 cm^{-1}, 6560 cm^{-1}and 7008 cm^{-1}) decreased with increasing lyophilization time.

Comparison of spectra from wet and dry shows that with serial lyophilization, there was a reduction in water absorbances at 5184 cm^{-1} and 7008 cm^{-1} but at 48 hours, features in those regions were still present; in contrast, only a negligible absorbance was observed at the 6560 cm^{-1} water absorbance. Therefore, the 6560 cm^{-1} water absorbance is suggested to arise from loosely bound water that can be fully removed with lyophilization, whereas the water absorbances at 5184 cm^{-1} and 7008 cm^{-1} have loosely and tightly bound water components, since the peaks reduce in intensity, but are still present with increasing lyophilization time. Thus, all three water absorbances have a loosely bound component, and two have both loosely and tightly bound water components. Another possible interpretation is that there are matrix absorbances that underlie the water absorbances at 5184 cm^{-1} and 7008 cm^{-1}, and thus all three of the major water absorbances may be "loosely bound" only. Further studies involving deuterium exchange would enable a conclusive determination of this. Interestingly, the 6688 cm^{-1} matrix peak becomes increasingly significant as the 6560 cm^{-1} loosely bound water diminishes (Fig. 15c).

Creation of a Water Calibration Curve using an Optimal Spectral Data Collection Method

Dehydration of bone through lyophilization affected the water and matrix NIR absorbances. Univariate correlation analysis between gravimetric water content either alone or ratioed to a matrix peak and NIR water absorbances, 5184 ($R= 0.84$, $p<0.05$) ,7008 ($R= 0.63$, $p<0.05$), 5184/4608 ($R= 0.96$, $p<0.05$) and 7008/6688 ($R= 0.90$, $p<0.05$) showed a significant linear correlation between the two variables (Table 2). Additionally, multiple liner regression (MLR) models were developed to predict gravimetric water content using individual water and matrix absorbances. In both the MLR models the root mean square error (RMSE for prediction based on intensities of the second derivative peaks at 5184 + 4608 (R= 0.95, p<0.05, RMSE = 0.67, 8.90%) and 7008 + 6688 (R= 0.93, p<0.05, RMSE = 9.30%) were comparable.

Table 2: Univariate analysis of NIR water and matrix absorbances to gravimetric water content. Statistical significance was set at p<0.05.

Frequencies	Component	R-value	RMSE
5184 cm^{-1}	water	0.84, p<0.05	12.50%
7008 cm^{-1}	Water	0.63, p<0.05	16.8%
5184/4608	Water/Matrix	0.96, p<0.05	9.90%
7008/6688	Water/Matrix	0.90, p<0.05	18.6%
5184 cm^{-1} + 4608 cm^{-1}	Water +Matrix	0.95, p<0.05	8.90%
7008 cm^{-1} + 6688 cm^{-1}	Water + Matrix	0.93, p<0.05	9.30%

PLS models were developed to correlate NIR spectral data to gravimetrically-determined water content. As seen in the scores plot (Fig. 16a), 92% of the variance among samples was primarily attributable to the changes in the water absorbance at 5184 cm^{-1} in factor 1 of the loadings plot. Additionally, factor 2 was dominated by matrix peaks, which influenced ~ 5% of the variance in the data (Fig. 16b).

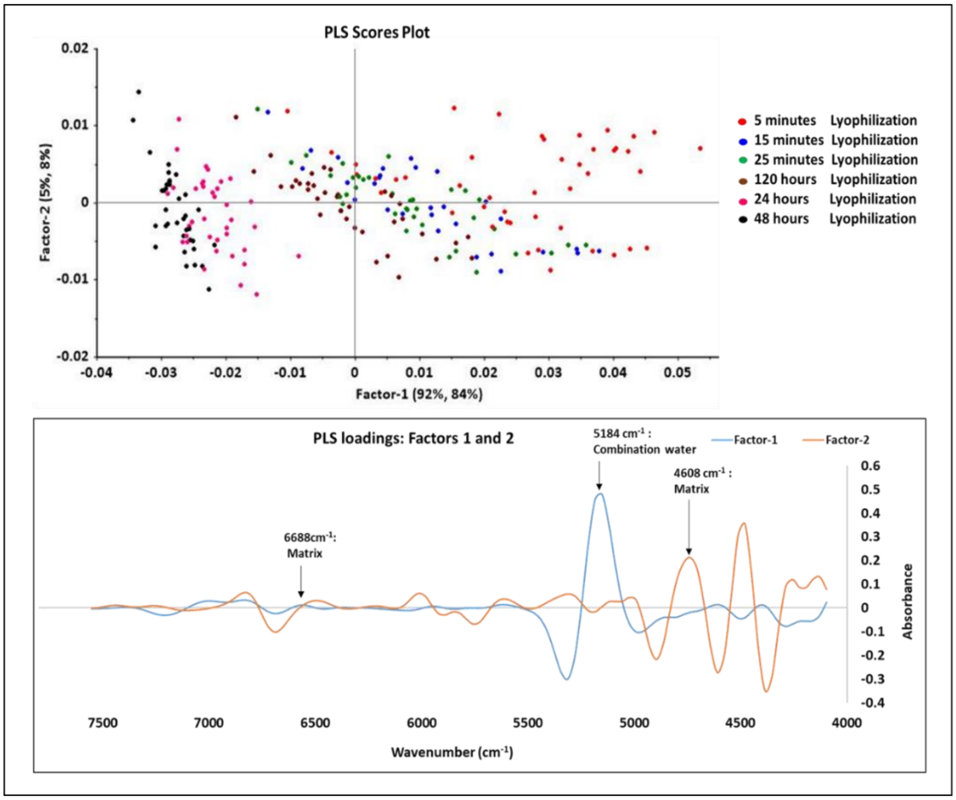

Figure 16: Top: The lyophilization time points separate from right to left, reflective of increasing lyophilization time. Bottom: factor 1, which underlies most of the data separation, is dominated by the 5184 cm^{-1} water absorbance, while factor 2 is dominated by matrix absorbances.

Three independent prediction models were developed that predicted water content with an average RMSEP of 7.39% of total water content. A significant correlation was seen between gravimetric and NIR-predicted water content in both the overall range of 0-10 % wet weight ($R= 0.96$, $p<0.05$, RMSEP = 0.67, 7.39%) (Fig. 17a) and in the physiologic range of 4-10% ($R=0.87$, $p< 0.05$, RMSEP = 0.81,14.5%) (Fig. 17b).

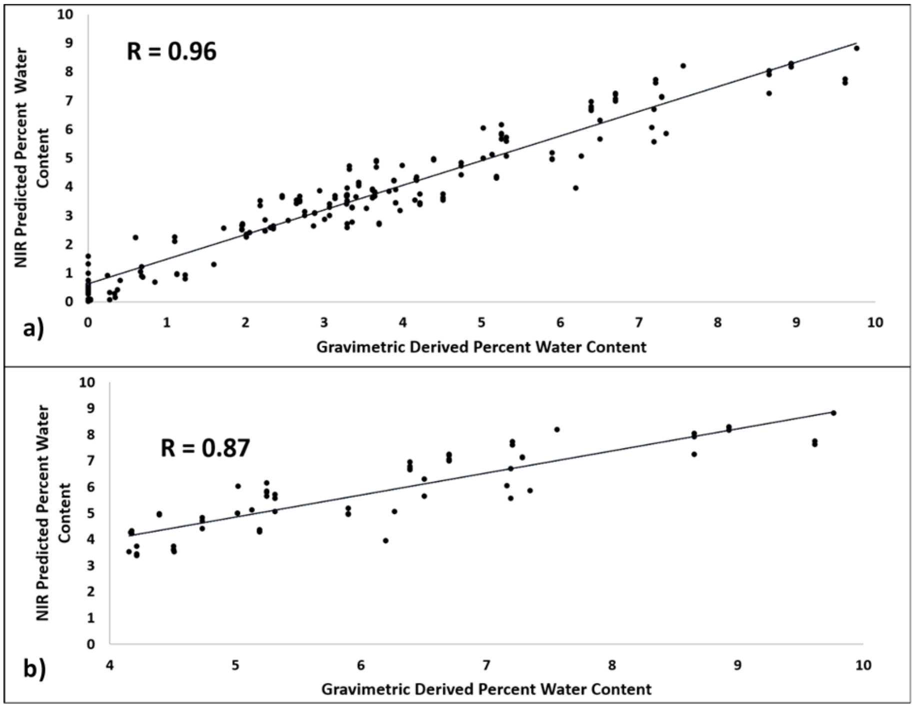

Figure 17: Independent NIRSI prediction of gravimetric water in cortical bone over the a) 0 -10 %, and b) 4-10% (physiologic) water content ranges. RMSEP for the two models 0-10% range and 4-10% range are 7.39% and 14.5% respectively.

Interestingly, the RMSECV value (6.60%) for the best PLS model (Table 2 and 3) was lower but in a similar range as the errors of the MLR models (5184 cm^{-1}+ 4608 cm^{-1} = 8.90%, 7008 cm^{-1} + 6688 cm^{-1} = 9.30%).

Table 3: Multivariate analysis PLS of NIR spectral data to gravimetric water content.

R-value	RMSECV
0.92, p<0.05	6.60%

3.5 Discussion

The current study demonstrates optimal conditions for collection of NIRSI data for evaluation of water from bone samples. Such methodology will be helpful for evaluation of changes in water in harvested pre-clinical samples from aging studies, and bone quality changes in therapeutic protocols. Clinically, bone mineral density (BMD) is considered the conventional technique for assessment of bone quality, which is related to bone strength, fracture risk and fragility [21, 40, 110]. However, BMD alone is not the sole indicator for fracture risk assessment. For example, changes in bone microarchitecture, cellular density, tissue organization, and compositional changes related to mineral and collagen water interactions can play a role in bone quality [1, 21, 111]. A recent study showed that BMD as an indicator accurately predicted only 50% of fractures[112], and it had only a weak correlation to bone strength. This motivates researchers to investigate additional biomarkers that can be used as indicators for bone quality assessment [40, 110, 113, 114].

Compositional changes in cortical bone after the age of 30 result in a gradual decrease in bone mass and an increase in bone fragility [1, 30, 32, 115]. Aging can trigger the displacement of collagen-associated water molecules due to increased glycation of crosslinking in collagen fibers [27]. Additionally, mineralization tends to decrease with age due to imbalances in the turnover process between bone resorption and formation [1]. Continuous bone loss with age leads to osteoporosis which is caused by a significant decrease in bone mass and an increase in bone porosity [32]. These compositional changes also decrease the structural integrity of cortical bone. Nyman et al. [85, 116, 117] performed extensive mechanical studies on bovine cortical bone and have shown that dehydration significantly decreases toughness, while stiffness increases [116, 117]. Collagen provides the toughness in cortical bone via its inter and intra molecular bonding to water molecules; These studies indicate that in dehydrated bone, longitudinal contraction increases for collagen and the fibrils become stiffer leading to a greater risk of bone fracture [85].

Anti-resorptive drugs used to treat osteoporosis such as Raloxifene act by binding to estrogen molecules to slow down the bone resorption process [118]. Gallant et al.[40] have shown that Raloxifene-treated beagles had a 17% percent increase in cortical bone water without significantly altering tissue BMD levels. They also found that Raloxifene had a positive effect on increasing bound water at the collagen/mineral interphase which effectively caused an increase in the overall bone toughness. This study along with several others emphasize that the hydration of bone correlates with bone mechanics better than BMD levels[15], [18], [119]. Together, these studies concluded that toughness significantly decreases with age and with dehydrating bone. Therefore, there is a strong possibility that bone water content can be used as an indicator for bone quality assessment.

Several studies have investigated cortical bone water through MRI and spectroscopic techniques for assessment of bone compositional integrity [18, 29, 56, 91, 110, 120, 121]. Rajapakse et al.[27] have previously suggested that 60% of the water content detected in cadaveric samples by UTE-MRI is associated with collagen bound water, while the remainder is pore-associated water. Additionally, studies in bovine cortical bone have also determined that 73% of water that is detected is collagen bound [18]. Chen et al. [121] showed that the ratio of free to bound water increases with the progression of osteoporosis, Allen et al. [118] through UTE-MRI analysis found that Raloxifene treated beagles had 14% more bound water compared to control samples. Clearly, changes in bone water can provide insight into disease progression and therapeutic effectiveness in bone-related diseases.

Unal et al. [91] also concluded that Raman spectroscopy is a feasible technique for determination of water content in tissues. In their study, they performed sequential dehydration experiments on bovine cortical bone and assigned water compartments for bone based on changes in Raman sub-bands under the broad OH-stretch. The data collection of dehydrating tissues took place in atmospheric conditions, with data collection time limited to 10 seconds per sample. While this method is feasible for wet samples, atmospheric water tends to infiltrate pores in lyophilized bone and may interfere with data collection and interpretation. In a recent study from our lab, we initially collected NIRSI data from 500-micron thick bone samples between two glass slides to minimize water loss during data collection [27]. However, atmospheric conditions could potentially interfere with data interpretation of serial dehydration and water calibration spectral imaging studies.

Accordingly, one main goal of the current study is to describe the importance of utilizing an environmentally-controlled chamber to assess water in cortical bone with NIRSI. NIR spectra are dominated by two previously reported water absorbances at 5184 cm^{-1} and 7008 cm^{-1} ,and one newly identified water peak at 6560 cm^{-1} [27]. The slow dehydration of bone over time helped to elucidate an absorbance at 6688 cm^{-1} that arises from N-H stretching in matrix molecules, along with the 4608 cm^{-1} absorbance that was previously established as a matrix absorbance [77]. Serial lyophilization of bone aided in classification of NIR water absorbances as either loosely or tightly bound. Data collection in atmospheric settings affects the repeatability of studies as atmospheric moisture can accumulate on the surface of sample, or conversely, if in a dry environment, can result in water evaporation during data collection. The sensitivity of NIR spectra to water is well known, and it was essential to collect data in an environmentally-controlled chamber that has a constant flow of low humidity for reliable measurements of compositional components without the interference of external water for dehydrated samples. However, in the future, if NIR data are being collected from hydrated samples, one can use either a chamber with high RH, or a chamber with low RH humidity, with the low RH data collection contingent on a short data collection time.

Analysis of second derivative peak heights of water and matrix showed the first significant reduction in water absorbance occurred after 120 minutes of lyophilization. (Fig. 15b). Since the 6560 cm^{-1} peak becomes insignificant with 48 hours of dehydration, it is suggested that after this timepoint any remaining water absorbances reflect tightly bound species. Additionally, since NIR spectra are dominated by water absorbances, the matrix peaks are better resolved with increasing dehydration time of the sample. For example, as the intensity of the 6560 cm^{-1} and 7008 cm^{-1} water peaks reduce, the adjacent matrix peak at 6688 cm^{-1} increases (Fig. 15b). Future studies will investigate the exact nature of the location of tightly bound water.

Both univariate and multivariate analysis were used to evaluate the spectral data. NIR inverted second derivative peak heights at 5184 and 7008 cm^{-1} significantly correlated with gravimetrically-derived water content (Table 2). Additionally, MLR models successfully predicted gravimetric water content by using inverted second derivative peak heights values of water and matrix absorbances.

PLS models showed strong correlations ($R = 0.92$) between NIR spectra and gravimetrically-derived percent water content. Factor 1 in the loadings plot clearly shows that the variation in the spectra related to water content arises from the water absorbances. Interestingly, factor 2 shows that after the water components, the matrix peaks influence the NIR spectral data as well. The correlation between spectral and gravimetric data in the physiologic range of 4-10% was somewhat lower ($R = 0.86$) compared to the full range data, in large part due to greater variation in the more hydrated tissues. One possible explanation is that residual surface water could still be evaporating during gravimetric data collection. Additionally, the rate of evaporation among the samples could have varied since some samples had larger surface areas compared to others, dependent on the exact porosity and area of the tissue.

As seen in Table 2 and 3, the errors obtained from the MLR and PLS models are comparable. Therefore, similar accurate results can be obtained by using both techniques to quantity spectral data. However, the advantage of using PLS regression, as opposed to single or two frequency NIR correlations, can be found across the entire range of spectral frequencies. Thus, additional frequencies that contribute to prediction of the outcome data could be identified. Additionally, PLS describes the data by grouping samples based on similar characteristics (chemical and physical). As seen in Tables 2 & 3, multivariate analysis error is lower than that from single peak analysis. Additionally, the loading plots in PLS models help to explain the variance that is seen in the entire data set. As observed in factor 1 and 2, the variation in the data set could be attributed to both changes in water and matrix absorbances at several frequencies.

As previously reported, the sensitivity of NIR to PO_4 absorbances is very low compared to what is observed in the mid-infrared region, and thus the mineral phosphate component cannot be identified by these combinations or overtones vibrations. However, P-OH overtone vibrations originating from mineral crystals in synthetic and biological powders have been assigned to ~7000 cm^{-1} [71], which could be useful for mineral assessment in bone. These findings need to be further validated to accurately identify peak positions, in particular intact bone tissues. It will be important to differentiate the OH vibrations originating from the apatite core from OH vibrations from water molecules bound to mineral.

Although the environmental chamber provided a stable environment in which to collect NIR data, this can also be considered a limitation of such studies. If this non-destructive technique for water assessment is to be truly useful in pre-clinical, or eventually clinical studies, it will be necessary to develop a method for data collection in atmospheric conditions. This would have to involve data collection in a limited time frame, to significantly reduce loss of water to the atmosphere, and may involve development or application of new instrumentation. Another limitation in transfer of this protocol to other samples is that here, all data collections were done using one spectrometer on samples of a uniform thickness. It is likely that the spectral processing techniques will have to be optimized with every data set acquired at different sample thicknesses, and possibly for data acquired with different spectrometers. For in vivo assessments, it is conceivable that a NIR method would be developed where water content relative to the amount of matrix present could be evaluated instead of absolute water content could be more useful.

In conclusion, we have developed a method to collect NIR spectral imaging data from dehydrating cortical bone samples in an environmentally-controlled chamber, which allowed for consistent measurements of bone water, and correlation of gravimetric and spectral data by PLS analysis to generate a water calibration curve. Further, future studies can continue to develop NIR water and matrix absorbances as potential biomarkers to provide insight into cortical bone quality by elucidation of the role of changes in water binding to collagen. Together NIRSI and appropriate analyses can shed light into primary molecular differences that can provide a foundation for development of techniques to assess compositional changes in bone with aging, disease states, and therapeutics.

CHAPTER 4: NEAR INFRARED SPECTROSCOPIC ASSESSMENT OF CORTICAL BONE WATER AS A POTENTIAL BIOMARKER FOR BONE QUALITY

Chapter 4 is a manuscript in preparation for submission to the Journal of Bone Mineral and Research. This study describes the elucidation of NIR water absorbances loosely and tightly bound to collagen and mineral, as well as NIR mineral absorbances. Additionally, the identified NIR water absorbances were correlated to structural properties in human cadaveric cortical bone samples. The studies in Chapter 4 pertain to Aims 2B, 2C and 3.

4.1 Abstract

Standard methods for evaluation of bone quality and prediction of related fracture risk have limitations, and thus identification of additional bone biomarkers is critical. Water is an important component of bone and plays a key role in its mechanical and structural integrity. Water molecules in bone are located in different compartments, either loosely bound to the tissue, or tightly bound to collagen and/or mineral. Here, we used near infrared (NIR) spectroscopy to identify different types of water present in bone, as well as to evaluate the potential of this technique as a non-destructive approach for assessment of bone mineralization and quality. Using a variety of carefully designed approaches, we successfully demonstrated that NIR spectroscopy is an effective tool to evaluate cortical bone water. In hydrated samples, NIR spectra have two main water absorbances at frequencies of ~5200 and 7000 cm^{-1}. Using lyophilization and hydrogen-deuterium exchange assays, we showed that these absorbances are primarily associated

with loosely bound bone water. However, using further demineralization assays, thermal denaturization, and comparison to standards, we found that these absorbances have underlying components associated with water molecules tightly bound to collagen (5170 cm^{-1}) and mineral (5225 and 7000 cm^{-1}). We also quantified the mineral-bound water as marker for bone mineral, demonstrating significant positive correlations between the NIR mineral absorbances and the mineral content as determined by established mid infrared spectroscopic parameters (phosphate/ amide I). Moreover, the NIR water absorbance data has potential to be used as a biomarker for bone properties, having correlation trends with tissue mineral density (TMD) in aging cadaveric cortical bone tissue. These observations reveal novel insights into the application of NIR spectroscopy to non-destructively identify bone water compartments, which may be valuable for pre-clinical and clinical studies of bone mineralization and quality.

4.2 Introduction

Cortical bone is a complex composite consisting primarily of hydroxyapatite (~70%), type 1 collagen (~20%) and water (~10%) [122]. Clinically-determined bone mineral density (BMD) is a key parameter that is widely used to assess bone quality, strength and fracture risk [25, 123]. However, studies have shown that BMD accounts for only 30-50% of fracture risk [21, 92, 123]. This has motivated research focused on determination of additional parameters that contribute to bone quality and fracture risk. One such potential contributor to bone quality is cortical bone water, which is found loosely and/or tightly bound to the bone mineral and collagen components [16, 27, 52]. In the current study, the term “loosely bound” refers to surface and interface water that can be removed through evaporation or lyophilization, whereas "tightly bound" water is trapped within the protein structure or mineral crystal lattice [15].

Bone tissue undergoes dynamic regeneration, where bone is continuously remodeled by formation and resorption processes. The quality of bone mechanical and structural properties are highly affected not only by changes in the mineral and collagen components, but also by the water compartments [22]. Bone water plays a crucial role in stabilizing collagen's triple helix through intra and inter molecular bonding [17], contributing to the mechanical properties of bone. Water present on the surface of the mineral also contributes to mechanical properties of bone by mediating the structuring and organization of the apatite crystals [124]. Recently, Nyman et al. [15, 63, 85, 116] extensively studied the effect of dehydration on the biomechanical properties of bone using the techniques of evaporation, and thermal and solvent dehydration on samples. They found that with age, the amount of bound water was reduced, and caused a related decrease in the overall bone toughness. Thus, it was concluded that bone hydration contributes to optimal biomechanical properties of mineralized collagen fibers. Studies have shown in small animal models that aging is correlated to an increase in the tissue mineral density (TMD) and a decrease in the total bound water content [15, 125].

Non-destructive modalities such as magnetic resonance (MR) imaging and vibrational spectroscopy (infrared and Raman) have been used to quantify the total amount of water in bone as well as to differentiate loosely and tightly bound bone water [27, 51, 83, 91, 125]. MR imaging can be used to detect collagen-associated water; however, due to a short T_2 signal, it is very difficult to assess mineral-related water content [18]. Infrared spectroscopy in the near infrared (NIR) region is known for its sensitivity to water [126]. NIR analysis has been previously used to not only differentiate between loosely and tightly bound water in musculoskeletal tissues such as cartilage, but also to identify key matrix and water absorbances in cortical bone [127, 128]. The two primary NIR cortical bone water absorbances occur at the frequencies of ~5200 and ~7000 cm^{-1} [27], where the former absorbance arises from a combination of O-H bending and stretching, while the latter arises from the O-H stretching first overtone. Recently, another NIR absorbance at 7000 cm^{-1} has been described as potentially arising from a structural OH vibration related to hydroxyapatite [71]. However, further studies are necessary to confirm if this absorbance is also associated with bone mineral, and in general, to determine how the NIR water absorbances can inform about the different environments of water in bone.

The present study uses several experimental approaches to identify and quantify NIR absorbances associated with loosely bound bone water, and with water molecules tightly bound to either collagen or mineral. We anticipate that the application of these NIR spectroscopic techniques will yield biomarkers for non-destructive assessment of bone quality in a variety of clinically relevant settings.

4.3 Method

Overall approach

Several different techniques (described in detail below) were employed to spectroscopically evaluate loosely-bound water, and water that is tightly-bound to either collagen or mineral in cortical bone (Fig. 18). The techniques included lyophilization, hydrogen/deuterium (H/D) exchange, demineralization, denaturation, and comparison to

NIR spectra of bone standards with different degrees of matrix mineralization, and comparison to NIR spectra of calcium phosphate standards with or without structural water. A typical NIR spectrum (frequency range 4000–12,000 cm^{-1}) consists of absorbances from overtones and combinations of mid infrared (MIR) fundamental vibrations (400–4000 cm^{-1}) of molecules with C-H, N-H and O-H moieties [77]. Changes in the NIR spectral contour of the two established cortical bone water absorbances at 5200 and 7000 cm^{-1} were analyzed in samples with known compositional differences, and conclusions were drawn to better understand how distinct types of bone water can be identified and quantified based on the NIR spectra.

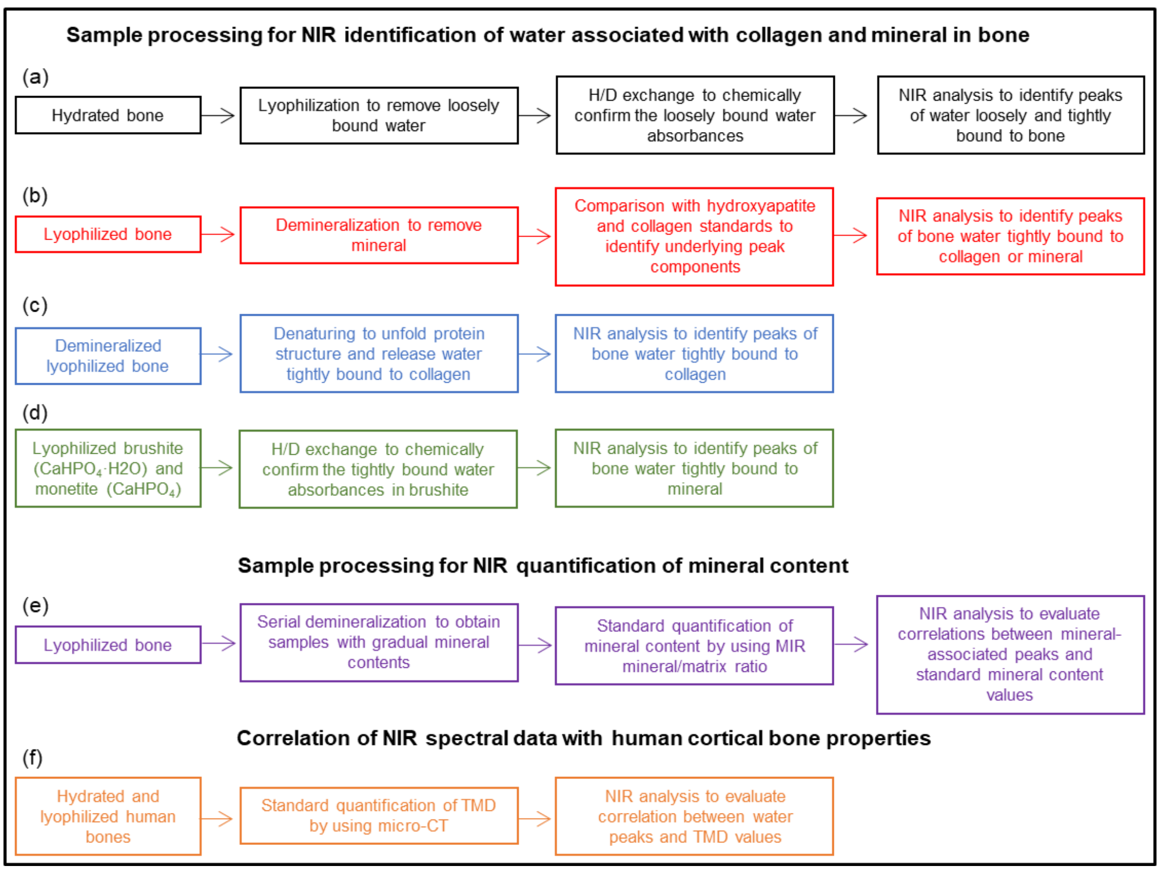

Figure 18: Flow chart of different approaches and techniques used to identify and to analyze NIR water peaks associated with collagen and/or mineral components of bone.

Sample processing for NIR identification of water absorbances associated with collagen and mineral in bone

Tightly bound collagen water

Removal of loosely bound bone water: All tissue samples were initially lyophilized in a lyophilizer (Martin Christ-Alpha 1-2) for 5 minutes to remove excess water. Five minutes of lyophilization was chosen to remove macroscopic surface water, and it also likely removed macroscopic pore water, which has been shown to correspond to a loss of 1.4-5.7 % of original bone mass [26]. The majority of the remaining loosely bound water was removed by lyophilization for 48 hours. To confirm that all loosely bound water was removed, lyophilized samples were subjected to H/D exchange by complete submersion in liquid D_2O (Sigma Aldrich, St. Louis) from 1 minute to 24 hours. H/D exchange is a chemical reaction of replacing available hydrogens with deuterium atoms in O-H, N-H or S-H bonds. This process would result in all freely available hydrogen ions in the native bone water exchanging with deuterium ions, resulting in the formation of X-D bonds. Since deuterium is a heavier isotope of hydrogen, we hypothesize that X-D bonds will vibrate at a lower NIR frequency compared to X-H bonds [129]. Thus, by investigation of NIR spectra of bone before and after soaking in deuterium, we can elucidate the type and location of bound water in NIR region. If there is no change in spectra after soaking in deuterium, there were no freely available hydrogens (water molecules).

Accordingly, it was concluded that the remaining spectral absorbances in the O-H absorbance regions after lyophilization and after subsequent H/D exchange originated from tightly bound water associated with either collagen and/or mineral.

Tightly bound collagen water: To specifically identify absorbances associated with water tightly bound to collagen, we used previously characterized demineralized porcine cortical bone samples [130]. The samples were lyophilized to remove loosely bound water and denatured at 75 degrees Celsius for two hours in an oven (Precision 658, Thermo Scientific). Denaturing unravels collagen's triple helix, exposing the tightly associated water molecules within the structure and loosening the water bonds to the protein [6]. Therefore, we hypothesized that the water tightly bound to collagen will be lost after denaturization, which could be observed as a decrease in the corresponding NIR water absorbance.

Tightly bound mineral water

To identify absorbances arising from water tightly bound to mineral, we investigated the NIR spectra of standard calcium phosphate compounds with and without structural water, brushite ($CaHPO_4 \cdot 2H_2O$) and monetite ($CaHPO_4$), respectively. The sole difference in their composition is the presence of tightly bound water. Brushite and monetite powders (Sigma Aldrich) were pressed into 100 mg pure pellets and lyophilized for 48 hours to remove loosely bound water. Following lyophilization, the samples underwent H/D exchange to ensure that any remaining water peaks observed in the spectra of brushite corresponded to tightly bound water molecules. We hypothesized that a NIR absorbance associated with bone mineral could be assigned to water tightly bound to the mineral if it corresponded to an absorbance in the O-H region present in the spectrum of brushite and absent in the spectrum of monetite.

Sample processing for NIR quantification of mineral content

To assess whether a mineral-associated absorbance from bone mineral is present in the NIR region, we compared the spectra of previously characterized mineralized and demineralized porcine cortical bone samples [130]. We hypothesized that removing mineral from bone would lead to a reduction in a mineral-associated absorbance, regardless of whether the absorbance arises directly from the mineral structure or from water tightly bound to mineral. The intensity of the potential mineral NIR absorbance was then evaluated for correlation with the MIR-determined mineral content of serially demineralized bone samples. For the mineral content experiments, tibiae from young bovine bone (Research 87) were pulverized (Spex Freezer/Mill 6770) to powder, and one gram of bone powder was mixed with 100 ml of 10 mM EDTA-Tris solution (Sigma Aldrich) and stirred together for one week with intermittent EDTA changes. The demineralization process was monitored by MIR assessment of aliquots of bone over a one-week period, and NIR data obtained from the lyophilized demineralized aliquots pressed into pellets (Carver Press 4350), as described below. We hypothesized that the successful identification of an NIR bone mineral absorbance would be marked by a strong positive correlation ($R>0.8$, $p < 0.05$) between a specific NIR absorbance and the MIR-determined mineral content of the bone samples.

Correlation of NIR spectral data with human cortical bone properties

We hypothesized that absorbances of specific NIR absorbance bands associated with mineral and/or matrix and/or water components correlate to age-related changes in human cortical bone tissue mineral density (TMD) determined by micro-computed tomography (micro-CT).

Tissue preparation for micro-CT

Cadaveric human tibiae harvested from 10% along the distal end from 6 female donors with no evidence of skeletal disease (NDRI, Philadelphia, PA) and were cut cross-sectionally to uniform 500 µm thick sections using a diamond wafering saw (Buehler Isomet 1000, Lake Bluff, IL). The sections were ultrasonicated (60 khz FS60D Fisher Scientific) for 120 minutes in 1% tergazyme detergent solution to remove bone marrow and stored in a solution of phosphate buffer solution (PBS) and protease inhibitor (PI) at -20°C until use. The sections were thawed and lyophilized for 5 minutes to remove remnant PBS/PI solution on the surface of the bone samples, and then weighed on SI 215D Denver Instruments Precision Balance (Bohemia, NY). Near infrared spectral imaging data (NIRSI) in an environmentally controlled chamber (described below) were collected prior to micro-CT imaging. Then, the bone sections were lyophilized for 48 hours prior to micro-CT data collection. This was done to avoid inconsistencies associated with water loss during micro-CT data collection. Sample water content for cadaver samples was calculated as the difference between weight at 5 minutes and 48 hours lyophilization. It was previously confirmed in a subset of 3 samples that micro-CT data parameters from wet and lyophilized samples did not differ, however (data not shown).

Micro-CT image acquisition and data analysis

Data from the lyophilized cortical bone cross-sections were obtained with a high-resolution cone-beam micro-CT scanner (SkyScan 1172; Bruker microCT, Kontich, Belgium) equipped with a Hamamatsu C9300 11Mp camera using the double-side and oversize sample options. The parameters used for micro-CT data collection were as follows: Source voltage, 62 kV; source current, 131 mA; 9.89µ pixel resolution, rotation step was 0.2°, 5 frames averaging, and random movement compensation was 10. The acquisition time for each sample was ~10 hours. The raw micro-CT images were reconstructed using cone-beam reconstruction software (SkyScan NRecon) with a ring artifact correction of 10, and a beam hardening correction of 60%. Next the images were rotated in the transverse direction using DataViewer software. In the rotated images, cortical bone only was selected as the volume of interest (VOI) region using a uniform threshold of 80 Hounsfield units (HU). Cortical bone TMD calibrated to known standards of CaHA of 0.25 and 0.75 g/ cm^{-3} 4 mm in diameter) were acquired from micro-CT images [131]. The calibration values were generated using custom processing algorithm on SkyScan CT Analyzer software (CTAn).

NIR spectroscopy data collection and analysis

NIR spectral data were obtained in diffuse reflectance mode using an ASD LabSpec 4 Standard-Res spectrometer coupled to a NIR fiber optic probe with a 3 mm tip diameter comprised of low-OH quartz fibers (Malvern Panalytical). Fifty co-added scans were collected with 1 nm spectral resolution and averaged, and ratioed to a background spectrum collected from a Spectralon reference standard. At least three spectra were collected from each sample and averaged. NIR raw spectra tend to have broad and overlapping absorbances, and therefore a second derivative filter (SavitzkyGolay, 2^{nd} order polynomial and 27 points of smoothing) was applied to NIR raw spectra to resolve underlying peaks. Several smoothing and filter algorithms were investigated initially, and this one ultimately resulted in the most reproducible data, with minimal noise and preservation of small absorbance peaks (data not shown). Second derivative peak height data have previously been shown to strongly correlate to integrated areas of absorbance bands, which reflect relative amounts of the components of interest [27]. Here, they are shown as inverted spectra, to display positive peaks.

An environmental sample chamber with an inflow of either dry air or deuterium vapor, dependent on the specific experiment, was used during NIR data collection [132]. Dry air was circulated inside the chamber during NIR data collection of lyophilized samples to prevent absorption of water from the environment. Deuterium vapor flow was supplied into the chamber during H/D exchange experiments to prevent exchange of deuterium ions back to hydrogen ions in the samples.

MIR data collection and analysis

MIR data from lyophilized mineralized and demineralized bone samples were acquired in attenuated total reflection (ATR) mode using a Thermo Scientific Nicolet iS5 spectrometer equipped with an iD7 ATR accessory with a diamond crystal. Spectra were collected with 4 cm^{-1} resolution and 32 co-added scans. At least three spectra were collected from each sample and averaged. The MIR raw spectra were baselined and normalized to amide I, the absorbance that arises from the protein components of bone, primarily collagen, for visualization of changes in mineral content. MIR spectral analysis of relative mineral content was based on the ratio of the second derivative peak heights of the primary phosphate peak, ~1200-900 cm^{-1}, arising from the asymmetric stretching of P-O bonds, to the amide I vibration of proteins which arises from carbonyl stretching (~1720-1585 cm^{-1}), termed the phosphate to Amide I ratio. This ratio has previously been shown to correlate to bone ash weight content [133].

MIR data collection and analysis

MIR data from lyophilized mineralized and demineralized bone samples were acquired in attenuated total reflection (ATR) mode using a Thermo Scientific Nicolet iS5 spectrometer equipped with an iD7 ATR accessory with a diamond crystal. Spectra were collected with 4 cm^{-1} resolution and 32 co-added scans from samples and from an air background. At least three spectra were collected from each sample and averaged. The MIR raw spectra were baselined and normalized to amide I, the absorbance that arises from the protein components of bone, primarily collagen, for visualization of changes in mineral content. MIR spectral analysis of relative mineral content was based on the ratio of the second derivative peak heights of the primary phosphate peak, 1200-900 cm^{-1}, arising from the asymmetric stretching of P-O bonds, to the amide I vibration of proteins which arise from carbonyl stretching (1720-1585 cm^{-1}), termed phosphate to amide I ratio. This ratio has previously been shown to correlate to bone ash weight content [133].

Statistical analysis

All spectral experiments were repeated twice. A Pearson correlation was used to evaluate the strength of a linear relationship in the data, with the R value reported, and a p-value < 0.05 considered to be statistically significant. Correlations were investigated between NIR peak heights and ratios and MIR-determined phosphate/amide I. Additionally, tissue mineral density was correlated to age of donor samples and to NIR-derived water content.

4.4 Results

NIR identification of water associated with collagen and mineral in bone

Analysis of the raw NIR spectra (Fig. 19a) and second derivative of the spectra (Fig. 19b) of hydrated, lyophilized and deuterated bone allowed differentiation of the primary water and matrix absorbances. Lyophilization of the samples led to a marked decrease in the absorbance intensities at 5200 and 7000 cm^{-1}, showing that they are primarily associated with loosely bound water in hydrated bone. This decrease in intensity is not observed in the matrix peak absorbances, such as the collagen absorbance at 4608 cm^{-1}[95]. There was, however, some intensity remaining in both primary water regions after lyophilization. H/D exchange was performed to confirm whether all loosely bound water was removed by lyophilization. Interestingly, the 7000 cm^{-1} absorbance had similar intensities in lyophilized and deuterated samples, but in the 5200 cm^{-1} region there was a small decrease in peak intensity, which indicated that lyophilization had not removed all the loosely bound water. Nevertheless, in both regions, at 5200 and 7000 cm^{-1}, absorbances remained after lyophilization and H/D exchange, indicating these peaks can be identified as water tightly bound to bone. The studies below then assessed which bone component the absorbances were associated with.

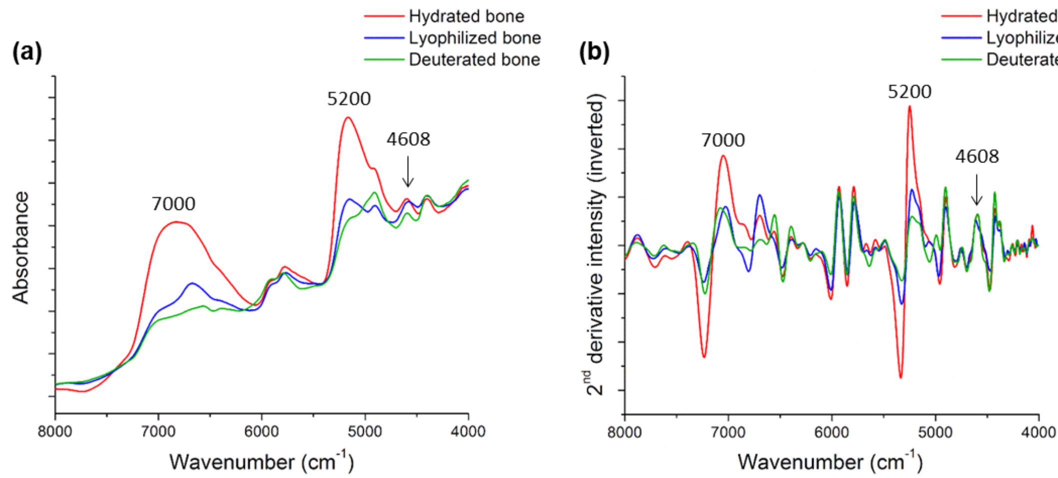

Figure 19: a) Raw and b) inverted second derivative bone spectra. Two main water absorbances are seen at 5200 and 7000 cm^{-1}. Lyophilization and H/D exchange show markedly lower peak intensities at the water absorbances, reflecting the that those peaks in hydrated samples are primarily associated with loosely bound water. In dehydrated samples, the peak remnants at the water regions are identified as water tightly bound to bone.

Bone samples were analyzed after demineralization to further understand whether the small peaks remaining at 5200 and 7000 cm^{-1} in lyophilized samples were related to water tightly bound to either collagen or mineral. Analysis of the second derivative of the spectra (Fig. 20a) shows that the peak at 7000 cm^{-1} is the only one that substantially decreases after demineralization, thus strongly indicating that this peak is primarily associated with bone mineral. Additionally, there was a noticeable shift of the 5200 cm^{-1} peak to a lower frequency with demineralization. Comparison this to NIR spectra of pure collagen and hydroxyapatite standards helped to identify underlying components of the 5200 cm^{-1} peak. It is clear that while the absorbance peak seen in bone has a maxima closer to that of hydroxyapatite at 5225 cm^{-1}, after demineralization, this peak position shifts and becomes similar to that observed in collagen at 5170 cm^{-1} (Fig. 20b). Therefore, we can conclude that the broad 5200 cm^{-1} absorbance in lyophilized bone has underlying components that arise from mineral (5225 cm^{-1} component) as well as from collagen (5170 cm^{-1} component).

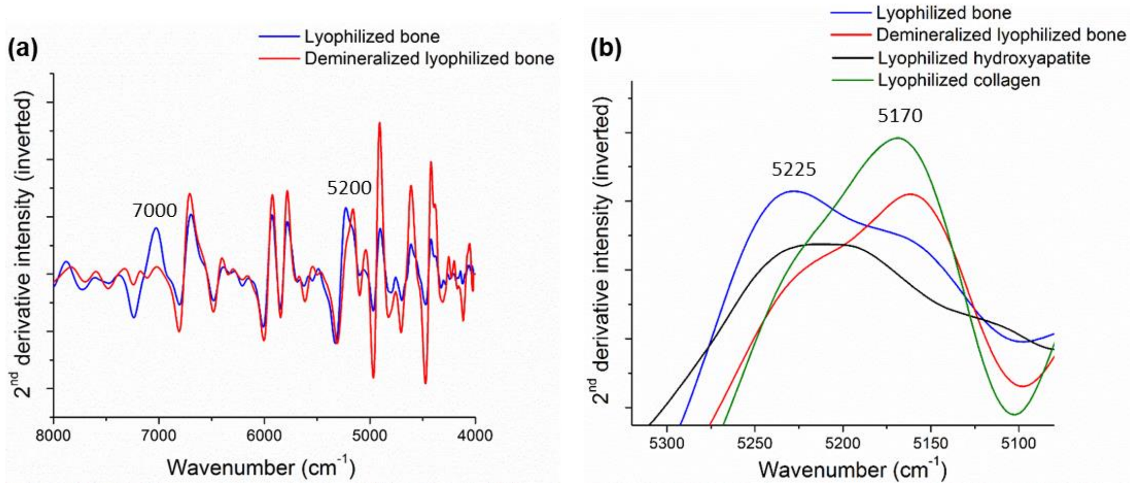

Figure 20: a) Inverted second derivative spectra of lyophilized and demineralized lyophilized bone. Demineralization of bone causes changes in spectral contour at only the two water absorbances. In particular, the peak at 7000 cm^{-1} is reduced, showing that it is clearly associated to the presence of bone mineral. The peak at 5200 cm^{-1} shows a noticeable shift. (b) Inverted second derivative spectra of bone, collagen and mineral standards. In dehydrated bone, two underlying components can be identified in the 5200 cm^{-1}peak region, which are primarily associated to collagen (5170 cm^{-1}) and mineral (5225 cm^{-1}).

To assess whether the 5170 cm^{-1} absorbance arises from water tightly bound to collagen, demineralized bone was denatured, aiming to disrupt the protein structure and loosen any water that was tightly bound to it. Analysis of the second derivative of the demineralized bone spectra (Fig. 21) after denaturation shows that only the 5170 cm^{-1} peak is substantially reduced after denaturing. This indicates that in lyophilized samples, this peak can be primarily identified as water tightly bound to collagen. The other absorbances in the NIR spectra of collagen are still present with denaturation.

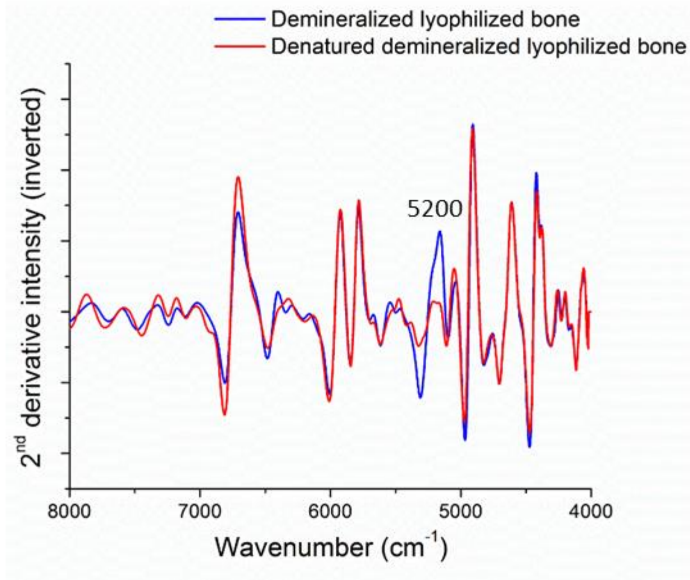

Figure 21: After denaturing demineralized bone, there is a pronounced decrease in peak intensity at ~5170 cm^{-1}water absorbance. This indicated that this peak in dehydrated samples is partially associated to water molecules tightly bound to collagen, which were lost after protein unfolding caused by denaturation.

As described above, the 7000 cm^{-1} and 5225 cm^{-1} absorbances in lyophilized bone are related to mineral. However, we sought to confirm the assignment of these peaks to a specific mineral-related molecular bond vibration by examination of the NIR spectra of mineral standards with and without structural water, brushite and monetite, respectively. The samples were lyophilized and subjected to H/D exchange to ensure observation only of tightly bound water peaks. Second derivatives of the spectra (Fig. 5) shows that while brushite has a clear absorbance peaks at 7000 cm^{-1} and 5225 cm^{-1}, these peaks are absent in monetite. The difference in spectra between monetite and brushite can only be attributed to structural water present in the composition of brushite. Therefore, we can identify the 7000 cm^{-1} and 5225 cm^{-1} peaks in lyophilized bone as water tightly bound to the mineral phase.

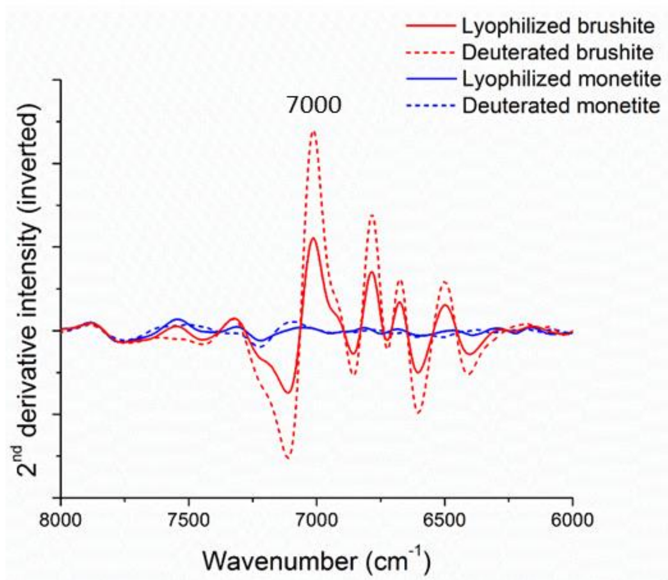

Figure 22: Comparing the spectra of brushite ($CaHPO_4 \cdot 2H_2O$) and monetite ($CaHPO_4$) shows that the peak at 7000 cm^{-1} arises from mineral structural water, present in brushite but not in monetite. H/D exchange confirms that this water is tightly bound to the mineral. This allows identifying the bone mineral absorbance seen in lyophilized samples at 7000 cm^{-1} as arising from water tightly bound to the mineral structure.

A summary of the loosely and tightly bound water absorbance peaks identified in hydrated and lyophilized bone is found in Table 4.

Table 4: Summary of the different types of water compartments identified by NIR in hydrated and lyophilized bone.

Frequencies	**Hydrated bone samples**	**Lyophilized bone samples**
~5200 cm^{-1}	Loosely bound water	Underlying peaks of ~5200 cm^{-1}: - 5170 cm^{-1} :Tightly bound water associated with collagen - 5225 cm^{-1} :Tightly bound water associated with mineral
~7000 cm^{-1}	Loosely bound water	Tightly bound structural water associated with mineral

NIR quantification of mineral content

NIR spectra are not sensitive to the primary phosphate mineral vibrations from phosphate [71], and thus to date have not been used to quantify mineral. However, it may be possible to use the above-described NIR peaks of structural water tightly bound to the mineral as a NIR biomarker to reflect the presence of bone mineral. Thus, we hypothesized that the NIR mineral-associated water peaks can be used to quantify bone mineral content. For this analysis, serially demineralized samples were evaluated, and MIR was used to obtain standard mineral content values, by quantifying the established phosphate/amide I peak ratio. Bone demineralization can be illustrated by the MIR raw spectra (Fig. 23a), which shows the relative decrease of the phosphate peak with progressive demineralization. In the second derivative of the NIR spectra obtained from lyophilized aliquots of progressively demineralized samples (Fig. 23b), both the 5200 and 7000 cm^{-1} absorbances also decreased in accordance with progression of demineralization over time.

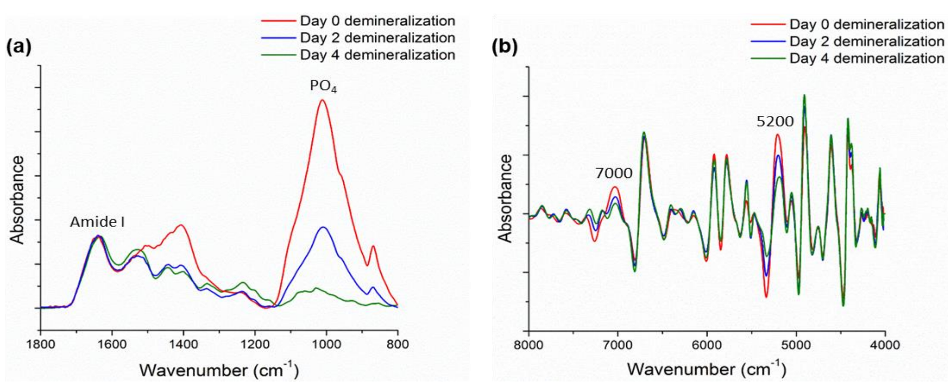

Figure 23: Serial demineralization of cortical bone seen after lyophilization in (a) raw MIR spectra and (b) NIR inverted second derivative spectra. MIR raw spectra shows that increasing demineralization leads to a decrease the phosphate absorbance. NIR analysis shows that both water absorbances at 5200 and 7000 cm^{-1}decrease with increasing demineralization, indicating that both peaks may be used as biomarkers of the presence of mineral in bones.

In serial demineralized lyophilized bone samples the 5200 cm^{-1} (Fig. 24a) and 7000 cm^{-1} (Fig. 24b) peak heights showed significant positive correlation to mineral content. It is interesting to note that the values obtained in the correlations are stronger with the 7000 cm^{-1} peak. This is most likely due to the observation above, that this peak is associated primarily with mineral, while the 5200 $cm^{-1}$is associated with both mineral and collagen components. In contrast, the collagen absorbance at 4608 cm^{-1} had a negative correlation with mineral content (Fig. 24c). These data clearly demonstrate that that the NIR absorbances deemed to be associated with mineral are indeed more present in mineralized samples, while the collagen-associated NIR absorbance peaks are more pronounced in demineralized samples. Accordingly, the ratios of the mineral peaks to the collagen peak also show significant positive correlation to MIR-determined mineral content, as shown in both the 5200/4608 ratio (Fig. 24d) and the 7000/4608 ratio (Fig. 24e). These results provide strong evidence that quantification of the peaks of water tightly bound to mineral at 5200 and 7000 cm^{-1} can be used to investigate mineral content.

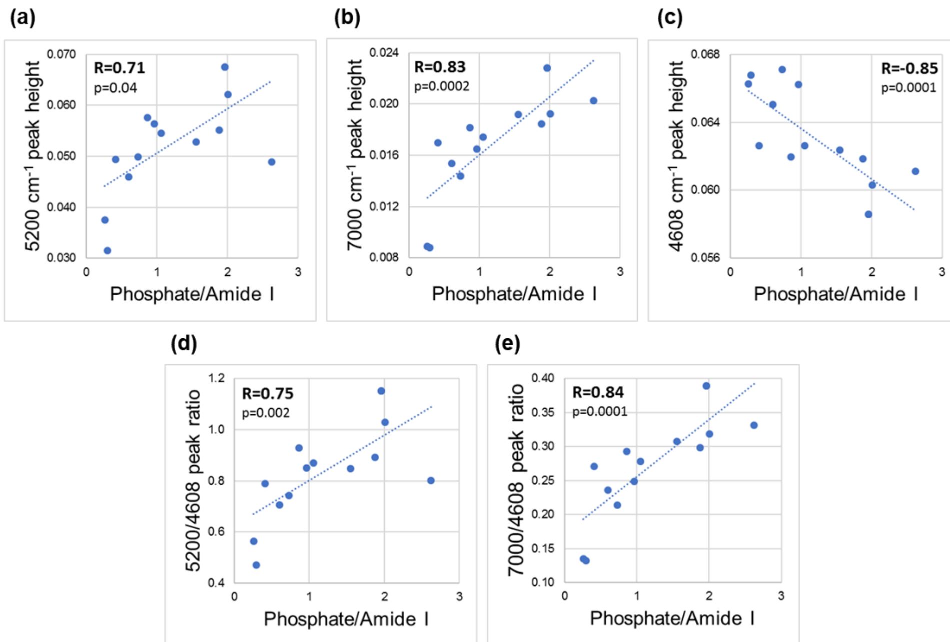

Figure 24: NIR absorbances of serially demineralized lyophilized bone correlated to MIR phosphate/amide I ratio, which represents mineral content. Individual peak heights at a) 5200 cm^{-1} and b) 7000 cm^{-1}had a significant correlation to mineral content, demonstrating the use of these peaks of water tightly bound to the mineral as biomarkers of bone mineral content. c) The collagen peak at 4608 cm^{-1} had a negative correlation to mineral content and can be used as a matrix peak to relative quantifications of mineral content. d) and e) NIR water/matrix ratios also show strong correlations to mineral content.

Correlation of NIR spectral data with human cortical bone properties

An interesting application of the NIR spectral analysis of absorbance peaks identified and quantified above may be for clinically relevant bone mineralization studies. In a series of female tibiae samples obtained from donors with a range of ages (Fig. 25), micro-CT determined TMD significantly correlated with donor age (Fig. 26a). Interestingly, in hydrated bones, quantification of the 5200/4608 peak ratio has a negative trend with increasing TMD (Fig. 26b), whereas, in lyophilized bones, the 7000/4608 peak ratio has a positive trend with TMD, although significance was not reached (Fig. 26c).

This suggests that with increasing tissue mineralization, total water content (combined loosely and tightly bound) decreases, while the specific water component tightly bound to the mineral increases, reflecting an increase in mineral content. A table of all correlations and trends can be found in the appendix section (Table 5). It is possible that increased sample size will further establish these relationships. Nevertheless, these preliminary results shed insights into the potential development of NIR approaches to non-destructively evaluate bone quality.

Figure 25: Micro-CT images of cross-sections of tibial bone from the youngest (33) and oldest (88-year-old) donors. Qualitatively, a decrease in cortical bone thickness with age is evident.

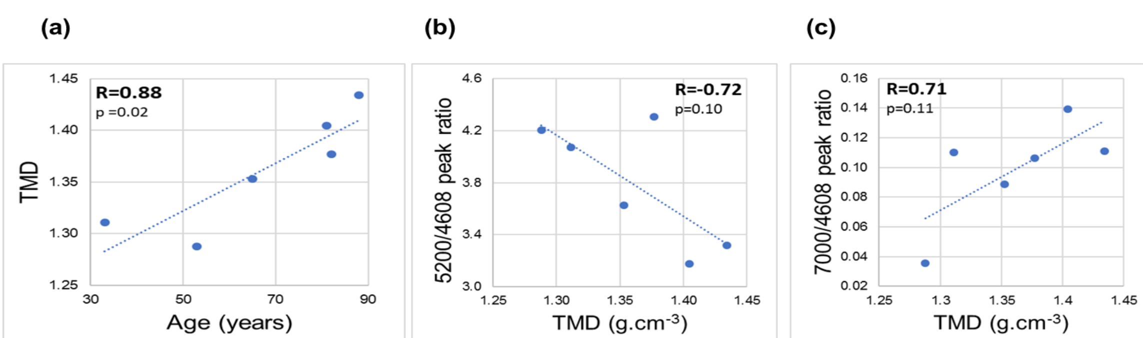

Figure 26: a) A strong and significant correlation was found between TMD and age of donors. b) In hydrated samples, quantification of overall water content tends to show a negative trend with TMD. c) In lyophilized samples, quantification of tightly bound mineral water has a positive trend with TMD. These indicate a potential application of NIR assessment of different bone water compartments to evaluate bone quality properties.

4.5 Discussion

It is well-known that clinically-determined BMD alone does not fully account for overall bone quality; therefore, factors such as bone hydration are being investigated as potential additional biomarkers to yield insight into bone strength and fragility [21, 22, 27, 125, 133]. The goals of the present study were twofold: to use NIR spectroscopy to identify and elucidate the various bone water compartments that are associated with collagen and mineral, and to correlate these identified NIR absorbances to compositional bone properties to better understand the role of water in bone quality. The results of this work present a significant contribution whereby this approach can now be used to fill a gap in the current knowledge of loosely and tightly bound water compartments in cortical bone. Moreover, a particular novelty of this work is the identification of a NIR absorbance assigned to bone mineral. Using the NIR peak of mineral-associated tightly bound water as a biomarker of bone mineral opens a promising window into the application of non-destructive approaches to evaluate bone properties in a large variety of clinically-relevant samples.

Non-destructive techniques such as MRI have helped discriminate bone water into two primary categories, free and collagen-bound. In MRI studies, free water is defined as water that is in the macroscopic and microscopic pores of bone tissues, and the remaining water, approximately 60-70% in cortical bone, is identified by NMR spectroscopy studies as collagen-bound water [18, 27]. However, this definition does not discriminate between water loosely and tightly bound to collagen. Further, an important limitation of these techniques is that they provide little information about mineral bound water, since the MR signal from mineral-bound water is too short to be identified and quantified. Therefore, this has motivated studies into other nondestructive and noninvasive techniques, such as vibrational spectroscopy (Raman and infrared) to evaluate bone hydration. Spectroscopic techniques have the ability to identify unique absorbances that can be used to quantify the amount of collagen, mineral and water in bone. Compared to MRI, vibrational spectroscopy can further elucidate and help to classify water compartments beyond just free and collagen-bound water. In this context, a key strength of the present study is the application of NIR spectroscopic approaches to allow a more specific detection and discrimination of water that is loosely and tightly bound to mineral and collagen. In the current study, loosely bound water comprised of ~8-10% of the total weight of the cadaver bone samples analyzed, which is in line with our previous studies where total bone water was evaluated [27, 131]. However, it's important to note that our definition of tightly bound water is not the same as that described in magnetic resonance studies. It is likely that the majority of the "collagen-bound" water described in MR studies is not tightly bound, and thus can be released with evaporation. Support for this is found in our negative trend of total water with bone age as found in our previous study [27], and the negative trend of total water with TMD found here, similar to the trends of MRI-determine collagen bound water with TMD and bone age.

Unal et al. have published studies based on the use of Raman spectroscopy to probe water compartments bound to collagen and/or mineral in cortical bone [16,56, 63]. Through serial evaporation and D_2O treatments on bovine cortical bone, they identified unique Raman absorbances that are associated with water loosely and tightly bound to both mineral and collagen, respectively [16]. Interestingly, in this study [56], unbound water was removed from cortical bovine samples by oven-drying drying samples at 40°C for 48 hours. The bound water was removed by submerging samples into ethanol for 36 hours to completely dehydrate the tissues. Both gravimetric water content and Raman spectra were collected throughout the removal of unbound and bound water. Prior to Raman spectral collection they performed a three-point bend test and measured the elastic modulus, toughness and strength of the samples. Additionally, porosity of the tissues was measured and used to correlate to Raman and gravimetric derived water content. They demonstrated that Raman-identified absorbances correlated to mechanical and structural bone properties [56]. They concluded that unbound water is directly correlated to increasing porosity. Raman derived water absorbances of unbound and bound correlated significantly to gravimetric derived unbound and bound water content respectively. Mineral bound water is primarily associated with the strength of the bone and collagen bound water is associated with bone toughness. Thus, that vibrational spectroscopic approach is clearly useful for assessment of bone quality however, the widespread availability, and high cost of the particular instrumentation required may impede widespread application of this technique.

Here, analysis of changes in the NIR spectra of hydrated, lyophilized and deuterated bone helped to confirm the two previously described water absorbances at 5200 and 7000 cm^{-1} [27]. We found that with removal of loosely bound water, these water absorbances significantly reduced in intensity, revealing underlying peaks related to tightly bound water in those spectral regions. Interestingly, comparing the NIR spectra of mineralized and demineralized bone as well as of denatured bone, collagen and mineral standards, we could further identify specific peaks associated with water compartments specifically tightly bound to collagen and mineral.

In the deuterated experiments, the accessibility of certain hydrogens to be readily exchange with deuterium atoms can yield insight into the various types of water compartments in bone tissue. For example, in collagen, the interlinking between collagen chains is caused by hydrogens that participate in hydrogen bonding between water molecules and amino acid side chains; these are labile hydrogens that can exchange with deuterium. However, hydrogen atoms located in the backbone of the collagen molecule that form intra-chain water bridges within in a single collagen chain will not exchange easily with deuterium. Therefore, in dehydrated bone, if there is a shift in NIR absorbances of O-H bonds to lower frequencies after H/D exchange, this indicates that those O-H bonds are now O-D bonds [129]. We presume that these arise from water molecules bound to collagen that are located in-between two collagen chains, known as “inter-chain”. If there are no shifts in frequencies of specific O-H absorbances after H/D exchange, then the hydrogens did not exchange with deuterium atoms and the O-H bonds were not altered. Therefore, these are hydrogens in water molecules that are tightly bonded and trapped within the collagen structure, or “intra-chain”. Similarly, in mineral, liable hydrogens in water molecules that are located on the surface of the crystals will exchange and become O-D bonds. Therefore, they will then vibrate at a lower frequency in the NIR region. If no exchange occurs, these O-H bonds are presumed to be located within the mineral crystal structure, known as “structural water”.

The 5200 cm^{-1} region was found to consist of absorbances from both mineral and collagen components. We found that in fully hydrated cortical bone samples, this peak arises from loosely bound water absorbances. However, with the removal of loosely bound water via lyophilization, this absorbance significantly reduces in intensity, shifts in peak position, and a shoulder on the main absorbance arises. In the lyophilized samples, the main peak maxima shifts to 5225 cm^{-1} , and this is identified here as a water-associated mineral absorbance, since it is similar to the peak position in stoichiometric hydroxyapatite, and showed a significant positive correlation with mineral content determined by the conventional MIR phosphate/amide I quantification. This shows that the absorbance at 5225 cm^{-1} in lyophilized bone sample originates from water associated with mineral and can be used for quantification of bone mineral.

After lyophilization of bone, the shoulder at 5170 cm^{-1} was proposed here to be water tightly bound within collagen. Comparing the spectra of the demineralized bone before and after denaturation, a substantial peak height reduction was observed in the demineralized denatured samples, indicating that the thermal treatment on the samples unraveled the helical collagen structure and exposed tightly bound water molecules that could then be released [6]. Hence, we show that the 5200 cm^{-1} absorbance has contributions from three distinct water compartments: loosely bound water absorbances can be identified in fully hydrated samples, whereas absorbances of tightly bound water to collagen and mineral are elucidated in lyophilized samples.

Studies have previously suggested the NIR absorbance at 7000 cm^{-1} as structural water [71] associated with mineral [27] ; however, since the mineral absorptivity is very low, this peak was not conclusively identified as related to mineral content. The present study is the first to quantify and define the water associated with mineral absorbances in the NIR spectral region. The reduction in the 7000 cm^{-1} absorbance after demineralization of bone samples confirmed that this peak indeed was related to mineral component vibrations. Additionally, the strong correlation observed between this NIR peak and the MIR phosphate/amide I ratio in serially demineralized samples further supported that the 7000 cm^{-1} absorbance can be assigned as a biomarker of bone mineral in dry samples. In hydrated bone, the 7000 cm^{-1} absorbance is a loosely bound water absorbance that overwhelms the mineral structural water absorbance. Interestingly, in Fig. 25a the MIR raw spectra shows that the carbonate absorbance at ~1400 cm^{-1} also decreases with increasing demineralization. Since both phosphate and carbonate reduce in peak intensity by day 4 of demineralization, this indicates that the carbonated apatitic mineral was successfully removed from bone.

Furthermore, calcium phosphates with and without structural water (brushite and monetite, respectively) were used as standards to help define the NIR absorbance at 7000 cm^{-1} as water tightly bound within the mineral crystal. It is important to mention that bone mineral is highly deficient in OH [135], and a resolved peak attributable to a structural OH absorbance is not present in the MIR spectrum [136]; therefore, the corresponding overtone and/or combination peak is also not observed in the NIR region. Mineral standards were subjected to H/D exchange to confirm that the water was tightly bound to the mineral, and not lost after exchange. With this approach, we observed that the 7000 cm^{-1} absorbance was strong in both the lyophilized and deuterated spectra of brushite, but negligible in that of monetite. This confirms that the 7000 cm^{-1} absorbance can be conclusively assigned to tightly bound structural water associated with mineral in lyophilized bone samples.

It is also interesting to discuss a potential application of the results obtained in this study to better understand the role of water in bone quality. A remarkable aspect of bone is the triple helical structure of collagen that acts as a scaffolding for water and mineral deposition. Aging triggers natural degradation of the organic matrix and an increase cortical bone TMD [137]. Tissue mineralization is related to the balance in the cellular remodeling process of bone resorption and formation via osteoclasts and osteoblasts respectively, and interestingly, age-related tissue mineralization increases have been associated with a decrease in overall bound bone water [138]. In addition, one study showed that in rodents, an increase in TMD was associated with an increase in collagen cross-linking and a reduction in collagen bound water. The results presented in the current study supports these findings, showing a trend between age and TMD in female cortical bone samples. Furthermore, we observed that with increased TMD, NIR quantification of the overall bone water (5200/4608) in hydrated samples decreases, whereas in lyophilized samples, the phosphate/amide I ratio (7000/4608) increases. Although, this data did not reach statistical significance for the small samples size available here (n=6), this can be highlighted as a potential application of NIR-determined water compartments as an alternative indicator for bone quality assessment. A strength of this modality, compared to MIR analysis, is the ability to analyze intact samples in pre-clinical studies. MIR studies generally required thin sample analysis, grinding samples into powders, or surface-only analysis using ATR. Additionally, NIR radiation has a greater depth of penetration (several millimeters to centimeters) into samples compared to MIR radiation. Further, the relatively low cost of NIR instrumentation may enable this approach for bone assessment to be widely accessible.

The ability to non-destructively to detect changes in cortical bone water and correlate to structural properties such bone density is still in the pre-clinical stages. Variations in tissue properties that surround bone also will effect the detection and elucidation NIR absorbances of water associated with collagen and mineral in clinical studies. A prospective study to transcutaneous analyze cortical bone with NIRS could be investigated as anatomical regions with little amounts of fat or skin, such as the tibia or metacarpals. The NIR water associated with collagen and mineral absorbances elucidated in this study can be used to approximate the potential frequencies that will be observed in clinical studies. Additionally, it is important note the structural organization of bone may vary according to the location, surrounding tissues and mechanical load it is subjected to.

The primary method of quantification of data in this study was by analysis of inverted second derivative peak height intensities of NIR absorbances, which can be dependent on spectral resolution. It is important to note that previously, Rajapakse et al.[27] concluded that inverted second derivative peak height intensities at 5200 and 7000 cm^{-1} water absorbances in NIR cortical bone spectra significantly correlated to integrated areas in raw data. To further confirm that the derivative is showing the same phenomenon as the raw data, an additional analysis could be performed on the spectra using multivariate curve resolution [139] or reconstruction [140]. There are many approaches to optimize these types of analyses, but one example of how we can apply this technique in our study is to reconstruct the lyophilized bone spectra in Fig. 20b from individual spectra of pure water, lyophilized collagen and mineral.

Limitations in this study include the difficulty in identifying water associated with a mineral absorbance in hydrated bone samples. NIRS sensitivity to water causes the spectra to be dominated by water absorbances throughout much of the range of interest. Therefore, the samples needed to be lyophilized to elucidate water-related mineral absorbances. Since there was a promising correlation between TMD and water content, a larger sample set could be investigated to better elucidate how NIR spectroscopy can contribute to understanding of age-related compositional changes in bone tissue.

In summary, we have demonstrated that NIR spectroscopic analysis of cortical bone can be used to identify water bound to different compartments: loosely bound to the tissue, tightly bound to collagen and tightly bound to mineral. This work presents a step forward in development of NIR spectral analysis for assessment of bone quality. Compared to MRI studies of bone water [18, 138], using a NIR approach allows for a more specific identification and classification of bone water. In particular, an important novelty of the current work is to apply NIR to identify absorbances of water tightly bound to bone mineral. We believe these absorbances may be of great value as a NIR biomarker of bone mineral content for pre-clinical or clinical assessment of bone quality, aiding in understanding the compositional changes that occur in cortical bone during aging and disease states.

CHAPTER 5: CONCLUSION

This thesis work helped to demonstrate that NIRS can be used as a sensitive tool to understand compositional changes that occur in aging bone. Additionally, the studies described above showed the applicability of NIR water absorbances as potential biomarkers for cortical bone quality assessment.

In Chapter one, an environmentally controlled chamber was designed and utilized to collect NIRSI spectral data from dehydrating cortical bone samples. Low RH humidity inside the chamber during NIR spectral collection was the optimal condition to collect reliable water measurements from dehydrating bone tissue. The two main bone water absorbances at 5184 cm^{-1} and 7008 cm^{-1} successfully correlated to gravimetrically-determined water content from bone. Additionally, both univariate and multivariate analysis of NIR spectral data revealed that with increasing lyophilization time of cortical bone, there was a decrease in water content, and an increase in matrix peak intensities at 4608 cm^{-1} and 6688 cm^{-1} accordingly. Interestingly, it was found that NIR inverted second derivative spectra acquired from bone could be used to successfully predict gravimetric water content with both MLR and PLS techniques.

Cortical bone water exists in different states. To effectively use the NIRS 5200 and 7000 cm^{-1} water absorbances as potential spectroscopic biomarkers for bone quality assessment, it is important to understand if these absorbances are associated with collagen or mineral. There are two main NIR water compartments in cortical bone loosely and tightly bound. In hydrated bone, both 5200 $cm^{-1}$and 7000 cm^{-1} absorbances arises from loosely bound water. Once cortical bone is dehydrated, the 5200 cm^{-1} absorbance shifts to approximately 5225 cm^{-1} and a shoulder arises on this peak at 5170 cm^{-1}. It was concluded that the 5170 cm^{-1} and 5225 cm^{-1} absorbances are water tightly bound to collagen and mineral respectively. Additionally, in dehydrated bone the 7000 cm^{-1} absorbance is tightly bound structural water associated with mineral in bone. The application of these identified water compartments to yield insights into structural properties such as TMD required investigation of their correlation with bone quality assessment. Interestingly, in hydrated bone samples loosely bound water at 5200 cm^{-1} had a negative trend with TMD, while in dehydrated tissues mineral bound water had a positive trend with age related increase in TMD. Therefore, mineral bound water increases with increase in total mineral content. Even though these correlations did not reach significance, it is a step forward to understand that NIRS could be a potential modality to efficiently to elucidate and differentiate the various bone compartments, which could aid in understanding changes in bone quality.

There are a few limitations to the studies described above. The data collected to generate the calibration curve described in Chapter 3 were from uniformly thick samples. The methodology and analysis as describe in Chapter 3 needs to be optimized for samples with varying thickness. NIR spectra is typically dominated with water, and in hydrated samples it was difficult to elucidate a mineral absorbance in wet bone tissue. Additionally, the identification of a mineral absorbance at 5225 cm^{-1} and 7000 cm^{-1} was only possible in dehydrated bone. In Chapter 4, the correlation of NIR water compartments to structural properties could be improved with the analysis of a larger sample set.

Notwithstanding these limitations, in summary, we have demonstrated that NIRS is an effective modality to detect bone's compositional absorbances that arise from water, collagen and mineral in bone. The primary novelty in this work is the identification of specific NIR water absorbances associated with collagen and mineral, which have been shown to have great potential as indicators for bone quality assessment.

REFERENCES

[1] A. Boskey and R. Coleman, “Aging and Bone,” *J. Dent. Res.*, vol. 89, no. 12, pp. 1333–1348, 2010.

[2] D. B. Burr and O. Akkus, *Bone Morphology and Organization*. Elsevier Inc., 2013.

[3] S. Weiner and H. D. Wagner, “The Material Bone: Structure-Mechanical Function Relations,” *Annu. Rev. Mater. Sci.*, vol. 28, no. 1, pp. 271–298, Aug. 1998.

[4] C. Gao, S. Peng, P. Feng, and C. Shuai, “Bone biomaterials and interactions with stem cells,” *Bone Res.*, vol. 5, p. 17059, Dec. 2017.

[5] X. Feng, “Chemical and Biochemical Basis of Cell-Bone Matrix Interaction in Health and Disease.,” *Curr. Chem. Biol.*, vol. 3, no. 2, pp. 189–196, May 2009.

[6] J. Bella, B. Brodsky, and H. M. Berman, “Hydration structure of a collagen peptide,” *Structure*, vol. 3, no. 9, pp. 893–906, 1995.

[7] K. Gelse, E. Pöschl, and T. Aigner, “Collagens-structure, function, and biosynthesis.”

[8] M. Geetha, R. Asokamani, J. Amit Kumar, and M. Ramalingam, “Mechanical characterization of nanofiber composites,” *Nanofiber Compos. Biomed. Appl.*, pp. 117–155, Jan. 2017.

[9] A. L. Boskey, “Noncollagenous matrix proteins and their role in mineralization,” *Bone Miner.*, vol. 6, no. 2, pp. 111–123, May 1989.

[10] R. W. Glanville, D. Breitkreutz, M. Meitinger, and P. P. Fietzek, “Completion of the amino acid sequence of the alpha 1 chain from type I calf skin collagen. Amino acid sequence of alpha 1(I)B8.,” *Biochem. J.*, vol. 215, no. 1, pp. 183–9, Oct. 1983.

[11] J.-Y. Rho, L. Kuhn-Spearing, and P. Zioupos, “Mechanical properties and the hierarchical structure of bone,” *Med. Eng. Phys.*, vol. 20, no. 2, pp. 92–102, Mar. 1998.

[12] M. J. Turunen, J. D. Kaspersen, U. Olsson, M. Guizar-Sicairos, M. Bech, F. Schaff, M. Tägil, J. S. Jurvelin, and H. Isaksson, “Bone mineral crystal size and organization vary across mature rat bone cortex,” *J. Struct. Biol.*, vol. 195, no. 3, pp. 337–344, Sep. 2016.

[13] C. Rey, C. Combes, C. Drouet, and M. J. Glimcher, “Bone mineral: update on chemical composition and structure.,” *Osteoporos. Int.*, vol. 20, no. 6, pp. 1013–21, Jun. 2009.

[14] B. Wopenka and J. D. Pasteris, “A mineralogical perspective on the apatite in bone,” *Mater. Sci. Eng. C*, vol. 25, no. 2, pp. 131–143, Apr. 2005.

[15] M. Granke, M. D. Does, and J. S. Nyman, “The Role of Water Compartments in the Material Properties of Cortical Bone,” *Calcif Tissue Int*, vol. 97, no. 3, pp. 292–307, 2015.

[16] M. Unal, S. Yang, and O. Akkus, “Molecular spectroscopic identification of the water compartments in bone,” *Bone*, vol. 67, pp. 228–236, 2014.

[17] J. Bella, B. Brodsky, and H. M. Berman, “Hydration structure of a collagen peptide,” *Structure*, vol. 3, no. 9, pp. 893–906, 1995.

[18] J. Chen, S. P. Grogan, H. Shao, D. D'Lima, G. M. Bydder, Z. Wu, and J. Du, "Evaluation of bound and pore water in cortical bone using ultrashort-TE MRI.," *NMR Biomed.*, vol. 28, no. 12, pp. 1754–1762, Dec. 2015.
[19] T. Sözen, L. Özışık, and N. Ç. Başaran, "An overview and management of osteoporosis.," *Eur. J. Rheumatol.*, vol. 4, no. 1, pp. 46–56, Mar. 2017.
[20] J. Compston, "Bone quality: what is it and how is it measured?," *Arq. Bras. Endocrinol. Metabol.*, vol. 50, no. 4, pp. 579–85, Aug. 2006.
[21] M. L. Bouxsein, "Bone quality: where do we go from here?," *Clin. Orthop. Relat. Res.*, vol. 14, pp. S118-27, 2003.
[22] H. et al. Fonseca, "Bone quality: the determinants of bone strength and fragility," *Sport. Med.*, vol. 44, no. 1, pp. 37–53, 2014.
[23] A. Khan, "Premenopausal women and low bone density.," *Can. Fam. Physician*, vol. 52, no. 6, pp. 743–7, Jun. 2006.
[24] E. M. Lewiecki and N. E. Lane, "Common mistakes in the clinical use of bone mineral density testing," *Nat. Clin. Pract. Rheumatol.*, vol. 4, no. 12, pp. 667–674, Dec. 2008.
[25] E. Donnelly, "Methods for Assessing Bone Quality: A Review," *Clin. Orthop. Relat. Res.*, vol. 469, no. 8, pp. 2128–2138, 2018.
[26] J. S. Nyman, L. E. Gorochow, R. Adam Horch, S. Uppuganti, A. Zein-Sabatto, M. K. Manhard, and M. D. Does, "Partial removal of pore and loosely bound water by low-energy drying decreases cortical bone toughness in young and old donors.," *J. Mech. Behav. Biomed. Mater.*, vol. 22, pp. 136–45, Jun. 2013.
[27] C. S. Rajapakse, M. V Padalkar, H. J. Yang, M. Ispiryan, and N. Pleshko, "Non-destructive NIR spectral imaging assessment of bone water: Comparison to MRI measurements," *Bone*, vol. 103, pp. 116–124, 2017.
[28] D. B. Burr and M. R. (Professor of anatomy and cell biology) Allen, *Basic and applied bone biology*. .
[29] G. S. Mandair and M. D. Morris, "Contributions of Raman spectroscopy to the understanding of bone strength," *Bonekey Rep*, vol. 4, p. 620, 2015.
[30] M. Saito and K. Marumo, "Collagen cross-links as a determinant of bone quality: a possible explanation for bone fragility in aging, osteoporosis, and diabetes mellitus," vol. 21, pp. 195–214, 2018.
[31] J. M. Kling, B. L. Clarke, and N. P. Sandhu, "Osteoporosis prevention, screening, and treatment: a review.," *J. Womens. Health (Larchmt).*, vol. 23, no. 7, pp. 563–72, Jul. 2014.
[32] "Osteoporosis prevention, diagnosis, and therapy," *Jama*, vol. 285, no. 6, pp. 785–795, 2001.
[33] W. F. Lems and H. G. Raterman, "Critical issues and current challenges in osteoporosis and fracture prevention. An overview of unmet needs," *Ther. Adv. Musculoskelet. Dis.*, vol. 9, no. 12, pp. 299–316, Dec. 2017.
[34] S. Migliaccio, M. Brama, and G. Spera, "The differential effects of bisphosphonates, SERMS (selective estrogen receptor modulators), and parathyroid hormone on bone remodeling in osteoporosis," 2007.
[35] E. G. Lufkin, M. Wong, and C. Deal, "The Role of Selective Estrogen Receptor

Modulators in the Prevention and Treatment of Osteoporosis," *Rheum. Dis. Clin. North Am.*, vol. 27, no. 1, pp. 163–185, Feb. 2001.

[36] A. Augoulea, E. Tsakonas, I. Triantafyllopoulos, D. Rizos, E. Armeni, N. Tsoltos, S. Tournis, E. Deligeoroglou, A. Antoniou, and I. Lambrinoudaki, "Comparative effects of denosumab or bisphosphonate treatment on bone mineral density and calcium metabolism in postmenopausal women."

[37] R. R. Recker and L. Armas, "The Effect of Antiresorptives on Bone Quality," *Clin. Orthop. Relat. Res.*, vol. 469, no. 8, pp. 2207–2214, Aug. 2011.

[38] C. T. Stringhetta-Garcia, S. R. L. Morais, F. Fernandes, M. J. Perez-Ueno, R. de P. Almeida, M. J. Q. Louzada, A. H. Chaves-Neto, E. Ervolino, and R. C. M. Dornelles, "Effects of strength training and raloxifene on femoral neck metabolism and microarchitecture of aging female Wistar rats," *Sci. Rep.*, vol. 7, no. 1, p. 14410, Dec. 2017.

[39] E. F. Calton, J. MacLeay, and A. L. Boskey, "Fourier Transform Infrared Imaging Analysis of Cancellous Bone in Alendronate- and Raloxifene-Treated Osteopenic Sheep," *Cells Tissues Organs*, vol. 194, no. 2–4, pp. 302–306, 2011.

[40] M. A. Gallant, D. M. Brown, M. Hammond, J. M. Wallace, J. Du, A. C. Deymier-Black, J. D. Almer, S. R. Stock, M. R. Allen, and D. B. Burr, "Bone cell-independent benefits of raloxifene on the skeleton: a novel mechanism for improving bone material properties.," *Bone*, vol. 61, pp. 191–200, Apr. 2014.

[41] S. Bose and A. Bandyopadhyay, *Materials and devices for bone disorders*. .

[42] S. Zaheer, M. LeBoff, and E. M. Lewiecki, "Denosumab for the treatment of osteoporosis.," *Expert Opin. Drug Metab. Toxicol.*, vol. 11, no. 3, pp. 461–70, Mar. 2015.

[43] E. I. Suvorova, P. P. Petrenko, and P. A. Buffat, "Scanning and Transmission Electron Microscopy for Evaluation of Order/Disorder in Bone Structure," *Scanning*, vol. 29, no. 4, pp. 162–170, Jul. 2007.

[44] G. Boivin, C. Anthoine-Terrier, and K. J. Obrant, "Transmission electron microscopy of bone tissue: A review," *Acta Orthop. Scand.*, vol. 61, no. 2, pp. 170–180, 1990.

[45] M. Georgiadis, R. Müller, and P. Schneider, "Techniques to assess bone ultrastructure organization: orientation and arrangement of mineralized collagen fibrils.," *J. R. Soc. Interface*, vol. 13, no. 119, 2016.

[46] D. C. Joy, "The theory and practice of high-resolution scanning electron microscopy," *Ultramicroscopy*, vol. 37, no. 1–4, pp. 216–233, Aug. 1991.

[47] G. C. Reilly, H. F. Knapp, A. Stemmer, P. Niederer, and M. L. Knothe Tate, "Investigation of the Morphology of the Lacunocanalicular System of Cortical Bone Using Atomic Force Microscopy," *Ann. Biomed. Eng.*, vol. 29, no. 12, pp. 1074–1081, Dec. 2001.

[48] N. Sasaki, A. Tagami, T. Goto, M. Taniguchi, M. Nakata, and K. Hikichi, "Atomic force microscopic studies on the structure of bovine femoral cortical bone at the collagen fibril-mineral level," *J. Mater. Sci. Mater. Med.*, vol. 13, no. 3, pp. 333–337, 2002.

[49] H. F. Knapp, G. C. Reilly, A. Stemmer, P. Niederer, and M. L. Knothe Tate,

"Development of preparation methods for and insights obtained from atomic force microscopy of fluid spaces in cortical bone.," *Scanning*, vol. 24, no. 1, pp. 25–33.

[50] P. J. Thurner, E. Oroudjev, R. Jungmann, C. Kreutz, J. H. Kindt, G. Schitter, T. Okouneva, M. E. Lauer, G. E. Fantner, H. G. Hansma, and P. K. Hansma, "Imaging of Bone Ultrastructure using Atomic Force Microscopy." 2007.

[51] S. P. G. Jun Chen Hongda Shao, Darryl D'Lima, Graeme M Bydder, M.B.Ch.B, Zhihong Wu Jiang Du, "Evaluation of Bound and Pore Water in Cortical Bone Using Ultrashort Echo Time (UTE) Magnetic Resonance Imaging," *NMR Biomed.*, vol. 28, pp. 1754–1762, 2015.

[52] C. Li, A. C. Seifert, H. S. Rad, Y. A. Bhagat, C. S. Rajapakse, W. Sun, S. C. Lam, and F. W. Wehrli, "Cortical bone water concentration: dependence of MR imaging measures on age and pore volume fraction," *Radiology*, vol. 272, no. 3, pp. 796–806, 2014.

[53] G. Katti, S. Arshiya Ara, and A. Shireen, "Magnetic Resonance Imaging (MRI)-A Review."

[54] H. H. Ong, A. C. Wright, and F. W. Wehrli, "Deuterium nuclear magnetic resonance unambiguously quantifies pore and collagen-bound water in cortical bone," *J. Bone Miner. Res.*, vol. 27, no. 12, pp. 2573–2581, Dec. 2012.

[55] W. Querido, J. M. Falcon, S. Kandel, and N. Pleshko, "Vibrational spectroscopy and imaging: applications for tissue engineering," *Analyst*, vol. 142, no. 21, pp. 4005–4017, Oct. 2017.

[56] M. Unal and O. Akkus, "Raman spectral classification of mineral- and collagen-bound water's associations to elastic and post-yield mechanical properties of cortical bone," *Bone*, vol. 81, pp. 315–326, 2015.

[57] M. D. Morris and G. S. Mandair, "Raman Assessment of Bone Quality," *Clin. Orthop. Relat. Res.*, vol. 469, no. 8, pp. 2160–2169, Aug. 2011.

[58] G. Keresztury, "Raman Spectroscopy: Theory," in *Handbook of Vibrational Spectroscopy*, J. M. Chalmers, Ed. Chichester, UK: John Wiley & Sons, Ltd, 2006.

[59] G. S. Bumbrah and R. M. Sharma, "Raman spectroscopy – Basic principle, instrumentation and selected applications for the characterization of drugs of abuse," *Egypt. J. Forensic Sci.*, vol. 6, no. 3, pp. 209–215, Sep. 2016.

[60] F. LaPlant, "Lasers, Spectrographs, and Detectors," Springer, Berlin, Heidelberg, 2010, pp. 1–24.

[61] B. H. Stuart, *Infrared Spectroscopy: Fundamentals and Applications*. Chichester, UK: John Wiley & Sons, Ltd, 2004.

[62] S. Kim, K. M. Byun, and S. Y. Lee, "Influence of water content on Raman spectroscopy characterization of skin sample," *Biomed. Opt. Express*, vol. 8, no. 2, p. 1130, Feb. 2017.

[63] M. Unal, A. Creecy, and J. S. Nyman, "The Role of Matrix Composition in the Mechanical Behavior of Bone," *Curr. Osteoporos. Rep.*, vol. 16, no. 3, pp. 205–215, Jun. 2018.

[64] B. Stuart, "Infrared Spectroscopy," in *Kirk-Othmer Encyclopedia of Chemical Technology*, Hoboken, NJ, USA: John Wiley & Sons, Inc., 2015, pp. 1–18.

[65] B. (Barbara H. . Stuart, *Infrared spectroscopy : fundamentals and applications*. J.

Wiley, 2004.
[66] P. R. Griffiths and J. A. De Haseth, *Fourier transform infrared spectrometry*. Wiley-Interscience, 2007.
[67] A. Boskey and N. Pleshko Camacho, "FT-IR imaging of native and tissue-engineered bone and cartilage.," *Biomaterials*, vol. 28, no. 15, pp. 2465–78, May 2007.
[68] W. Querido, R. Ailavajhala, M. Padalkar, and N. Pleshko, "Validated Approaches for Quantification of Bone Mineral Crystallinity Using Transmission Fourier Transform Infrared (FT-IR), Attenuated Total Reflection (ATR) FT-IR, and Raman Spectroscopy."
[69] C. Du and J. Zhou, "Evaluation of soil fertility using infrared spectroscopy: a review," *Environ. Chem. Lett.*, vol. 7, no. 2, pp. 97–113, Jun. 2009.
[70] C. Pasquini, "Near Infrared Spectroscopy: fundamentals, practical aspects and analytical applications," *J. Braz. Chem. Soc.*, vol. 14, no. 2, pp. 198–219, Apr. 2003.
[71] J. Kolmas, D. Marek, and W. Kolodziejski, "Near-Infrared (NIR) Spectroscopy of Synthetic Hydroxyapatites and Human Dental Tissues," *Appl Spectrosc*, vol. 69, no. 8, pp. 902–912, 2015.
[72] P. D. Jun Huang, P. D. Saly Romero-Torres, and Mojgan Moshgbar, "Practical Considerations in Data Pre-treatment for NIR and Raman Spectroscopy," 2010. .
[73] ÅsmundRinnanFrans van denBergSøren BallingEngelsen, "Review of the most common pre-processing techniques for near-infrared spectra," *TrAC Trends Anal. Chem.*, vol. 28, no. 10, pp. 1201–1222, Nov. 2009.
[74] H. Martens and E. Stark, "Extended multiplicative signal correction and spectral interference subtraction: new preprocessing methods for near infrared spectroscopy.," *J. Pharm. Biomed. Anal.*, vol. 9, no. 8, pp. 625–35, 1991.
[75] H. Mark, J. Workman, H. Mark, and J. Workman, "Derivatives in Spectroscopy: Part 2—The 'True' Derivative," *Chemom. Spectrosc.*, pp. 363–369, Jan. 2018.
[76] S. Saarakkala, L. Rieppo, J. Rieppo, and J. S. Jurvelin, "Fourier Transform Infrared (FTIR) Microspectroscopy of Immature, Mature and Degenerated Articular Cartilage."
[77] D. Burns and E. W. Ciurczak, *Handbook of Near-Infrared Analysis*, 3rd ed., vol. 35. CRC Publisher.
[78] U. P. Palukuru, A. Hanifi, C. M. McGoverin, S. Devlin, P. I. Lelkes, and N. Pleshko, "Near infrared spectroscopic imaging assessment of cartilage composition: Validation with mid infrared imaging spectroscopy," *Anal. Chim. Acta*, vol. 926, pp. 79–87, Jul. 2016.
[79] D. Burns and E. W. Ciurczak, *Handbook of Near- Infrared Analysis*, Third Edit. Boca Raton: CRC Publisher, 2001.
[80] A. Ural and D. Vashishth, "Interactions between microstructural and geometrical adaptation in human cortical bone," *J. Orthop. Res.*, vol. 24, no. 7, pp. 1489–1498, Jul. 2006.
[81] K. H. Barck, W. P. Lee, L. J. Diehl, J. Ross, P. Gribling, Y. Zhang, K. Nguyen, N. van Bruggen, S. Hurst, and R. A. D. Carano, "Quantification of cortical bone loss

and repair for therapeutic evaluation in collagen-induced arthritis, by micro-computed tomography and automated image analysis," *Arthritis Rheum.*, vol. 50, no. 10, pp. 3377–3386, Oct. 2004.
[82] H. M. BRITZ, J. JOKIHAARA, O. V. LEPPÄNEN, T. JÄRVINEN, and D. M. L. COOPER, "3D visualization and quantification of rat cortical bone porosity using a desktop micro-CT system: a case study in the tibia," *J. Microsc.*, vol. 240, no. 1, pp. 32–37, Oct. 2010.
[83] C. S. Rajapakse, M. Bashoor-Zadeh, C. Li, W. Sun, A. C. Wright, and F. W. Wehrli, "Volumetric Cortical Bone Porosity Assessment with MR Imaging: Validation and Clinical Feasibility," *Radiology*, 2015.
[84] A. C. Seifert, C. Li, C. S. Rajapakse, M. Bashoor-Zadeh, Y. A. Bhagat, A. C. Wright, B. S. Zemel, A. Zavaliangos, and F. W. Wehrli, "Bone mineral ^{31} P and matrix-bound water densities measured by solid-state ^{31} P and ^{1} H MRI," *NMR Biomed.*, vol. 27, no. 7, pp. 739–748, Jul. 2014.
[85] J. S. Nyman, A. Roy, X. Shen, R. L. Acuna, J. H. Tyler, and X. Wang, "The influence of water removal on the strength and toughness of cortical bone," *J. Biomech.*, vol. 39, no. 5, pp. 931–938, 2006.
[86] J. Yan, A. Daga, R. Kumar, and J. J. Mecholsky, "Fracture toughness and work of fracture of hydrated, dehydrated, and ashed bovine bone," *J Biomech*, vol. 41, no. 9, pp. 1929–1936, 2008.
[87] P. Zioupos and J. D. Currey, "Changes in the stiffness, strength, and toughness of human cortical bone with age," *Bone*, vol. 22, no. 1, pp. 57–66, 1998.
[88] J. W. Melvin, "Fracture mechanics of bone.," *J. Biomech. Eng.*, vol. 115, no. 4B, pp. 549–54, Nov. 1993.
[89] E. A. Zimmermann, B. Busse, and R. O. Ritchie, "The fracture mechanics of human bone: influence of disease and treatment," *Bonekey Rep.*, vol. 4, p. 743, Sep. 2015.
[90] R. Havaldar, S. Pilli, and B. Putti, "Insights into the effects of tensile and compressive loadings on human femur bone," *Adv. Biomed. Res.*, vol. 3, no. 1, p. 101, 2014.
[91] M. Unal, S. Yang, and O. Akkus, "Molecular spectroscopic identification of the water compartments in bone," *Bone*, vol. 67, pp. 228–236, 2014.
[92] D. B. Burr, "Changes in bone matrix properties with aging," *Bone*, vol. 120, pp. 85–93, 2018.
[93] A. Techawiboonwong, H. K. Song, M. B. Leonard, and F. W. Wehrli, "Cortical bone water: in vivo quantification with ultrashort echo-time MR imaging," *Radiology*, vol. 248, no. 3, pp. 824–833, 2008.
[94] M. D. Morris and G. S. Mandair, "Raman assessment of bone quality," *Clin. Orthop. Relat. Res.*, vol. 469, no. 8, pp. 2160–2169, 2011.
[95] U. P. Palukuru, A. Hanifi, C. M. McGoverin, S. Devlin, P. I. Lelkes, and N. Pleshko, "Near infrared spectroscopic imaging assessment of cartilage composition: Validation with mid infrared imaging spectroscopy," *Anal. Chim. Acta*, vol. 926, pp. 79–87, Jul. 2016.
[96] J. U. Porep, D. R. Kammerer, and R. Carle, "On-line application of near infrared

(NIR) spectroscopy in food production," *Trends Food Sci. Technol.*, vol. 46, no. 2, Part A, pp. 211–230, 2015.
[97] C. Haiyan and Y. He, "Theory and application of near infrared reflectance spectroscopy in determination of food quality," *Trends Food Sci. Technol.*, vol. 18, pp. 72–83, 2007.
[98] H. et al. Zhang, "Rapid, non-destructive determination of ginseng seed moisture content by near infrared spectroscopy technology," *Seed Sci. Technol.*, vol. 46, pp. 365–369, 2018.
[99] G. Reich, "Near-infrared spectroscopy and imaging: Basic principles and pharmaceutical applications," *Adv. Drug Deliv. Rev.*, vol. 57, no. 8, pp. 1109–1143, 2005.
[100] M. Jamrogiewicz, "Application of the near-infrared spectroscopy in the pharmaceutical technology," *J Pharm Biomed Anal*, vol. 66, pp. 1–10, 2012.
[101] H. Büning-Pfaue, "Analysis of water in food by near infrared spectroscopy," *Food Chem.*, vol. 82, no. 1, pp. 107–115, 2003.
[102] M. Padalkar and N. Pleshko, "Wavelength-Dependent Penetration Depth of Near Infrared Radiation into Cartilage," *Analyst*, vol. 140, no. 7, pp. 2093–2100, 2015.
[103] M. Padalkar, R. Spencer, and N. Pleshko, "Near Infrared Spectroscopic Evaluation Of Water In Hyaline Cartilage," *Ann Biomed Eng*, vol. 41, no. 11, 2013.
[104] M. Unal and O. Akkus, "Shortwave-infrared Raman spectroscopic classification of water fractions in articular cartilage ex vivo," *J. Biomed. Opt.*, vol. 23, no. 01, p. 1, Jan. 2018.
[105] P. Larkin, *Infrared and Raman Spectroscopy: Principles and Spectral Interpretation*. Elsevier.
[106] G. Chang, S. Boone, D. Martel, C. S. Rajapakse, R. S. Hallyburton, M. Valko, S. Honig, and R. R. Regatte, "MRI assessment of bone structure and microarchitecture," *J. Magn. Reson. imaging JMRI*, vol. 46, pp. 323–337, 2018.
[107] R. L. Carneiro and R. J. Poppi, "Infrared imaging spectroscopy and chemometric tools for in situ analysis of an imiquimod pharmaceutical preparation presented as cream," *Spectrochim. Acta Part A Mol. Biomol. Spectrosc.*, vol. 118, pp. 215–220, 2014.
[108] D. Dong and C. Zhao, "Limitations and challenges of using Raman spectroscopy to detect the abiotic plant stress response," *Proc. Natl. Acad. Sci.*, vol. 114, pp. E5486–E5487, 2017.
[109] H. J. Luinge, J. H. van der Maas, and T. Visser, "Partial least squares regression as a multivariate tool for the interpretation of infrared spectra," *Chemom. Intell. Lab. Syst.*, vol. 28, no. 1, pp. 129–138, 1995.
[110] R. Biswas, W. Bae, E. Diaz, K. Masuda, C. B. Chung, G. M. Bydder, and J. Du, "Ultrashort echo time (UTE) imaging with bi-component analysis: Bound and free water evaluation of bovine cortical bone subject to sequential drying," *Bone*, vol. 50, no. 3, pp. 749–755, 2012.
[111] R. B. Martin and J. Ishida, "The relative effects of collagen fiber orientation, porosity, density, and mineralization on bone strength," *J Biomech*, vol. 22, no. 5, pp. 419–426, 1989.

[112] A. Unnanuntana, B. P. Gladnick, E. Donnelly, and J. M. Lane, “The Assessment of Fracture Risk,” *J Bone Jt. Surg Am*, vol. 92, no. 3, pp. 743–753, 2010.
[113] C. R. Russo, F. Lauretani, S. Bandinelli, B. Bartali, A. Di Iorio, S. Volpato, J. M. Guralnik, T. Harris, and L. Ferrucci, “Aging bone in men and women: beyond changes in bone mineral density,” *Osteoporos Int*, vol. 14, no. 7, pp. 531–538, 2003.
[114] B. R. McCreadie and S. A. Goldstein, “Biomechanics of fracture: is bone mineral density sufficient to assess risk?,” *J Bone Min. Res*, vol. 15, no. 12, pp. 2305–2308, 2000.
[115] P. Zioupos, “Ageing human bone: factors affecting its biomechanical properties and the role of collagen,” *J Biomater Appl*, vol. 15, no. 3, pp. 187–229, 2001.
[116] J. S. Nyman, Q. Ni, D. Nicolella, and X. Wang, “Measurements of mobile and bound water by nuclear magnetic resonance correlate with mechanical properties of bone,” *Bone*, vol. 42, no. 1, pp. 193–199, 2008.
[117] X. Wang, R. A. Bank, J. M. Tekoppele, and C. M. Agrawal, “The role of collagen in determining bone mechanical properties,” *J. Orthop. Res.*, vol. 19, no. 6, pp. 1021–1026, Nov. 2001.
[118] A. M. R, T. PR, L. C, P. ersohn S, J. L, R. AA, M. BP, N. CL, B. DB, and H. GD, “In Vivo UTE-MRI Reveals Positive Effects of Raloxifene on Skeletal-Bound Water in Skeletally Mature Beagle Dogs,” *J. Bone Miner. Res.*, vol. 38, pp. 1441–1444, 2015.
[119] M. R. Allen, K. Iwata, M. Sato, and D. B. Burr, “Raloxifene enhances vertebral mechanical properties independent of bone density,” *Bone*, vol. 39, no. 5, pp. 1130–1135, 2006.
[120] M. D. Morris and G. S. Mandair, “Raman assessment of bone quality,” *Clin. Orthop. Relat. Res.*, vol. 469, no. 8, pp. 2160–2169, 2011.
[121] J. Du, “Magnetic Resonance Imaging of Bound and Free Water in Cortical Bone.”
[122] A. L. Boskey, “Bone composition: relationship to bone fragility and antiosteoporotic drug effects.,” *Bonekey Rep.*, vol. 2, p. 447, 2013.
[123] E. Seeman and P. D. Delmas, “Bone Quality — The Material and Structural Basis of Bone Strength and Fragility,” *N. Engl. J. Med.*, vol. 354, no. 21, pp. 2250–2261, May 2006.
[124] Y. Wang, S. Von Euw, F. M. Fernandes, S. Cassaignon, M. Selmane, G. Laurent, G. Pehau-Arnaudet, C. Coelho, L. Bonhomme-Coury, M.-M. Giraud-Guille, F. Babonneau, T. Azaïs, and N. Nassif, “Water-mediated structuring of bone apatite,” *Nat. Mater.*, vol. 12, no. 12, pp. 1144–1153, Dec. 2013.
[125] J. S. Nyman, S. Uppuganti, M. Unal, C. J. Leverant, S. Adabala, M. Granke, P. Voziyan, and M. D. Does, “Manipulating the Amount and Structure of the Organic Matrix Affects the Water Compartments of Human Cortical Bone,” *JBMR Plus*, Jan. 2019.
[126] C. Pasquini, “Near Infrared Spectroscopy: fundamentals, practical aspects and analytical applications,” *J. Braz. Chem. Soc.*, vol. 14, no. 2, pp. 198–219, Apr. 2003.
[127] M. Padalkar, R. Spencer, and N. Pleshko, “Near Infrared Spectroscopic Evaluation

Of Water In Hyaline Cartilage."
[128] U. P. Palukuru, A. Hanifi, C. M. McGoverin, S. Devlin, P. I. Lelkes, and N. Pleshko, "Near infrared spectroscopic imaging assessment of cartilage composition: Validation with mid infrared imaging spectroscopy," *Anal Chim Acta*, vol. 926, pp. 79–87, 2016.
[129] M. Unger, Y. Ozaki, and H. W. Siesler, "Variable-Temperature Fourier Transform Near-Infrared Imaging Spectroscopy of the Deuterium/Hydrogen Exchange in Liquid D2O," *Appl. Spectrosc.*, vol. 68, no. 5, pp. 603–607, May 2014.
[130] J. Wischmann, F. Lenze, A. Thiel, S. Bookbinder, W. Querido, O. Schmidt, R. Burgkart, R. von Eisenhart-Rothe, G. H. S. Richter, N. Pleshko, and P. Mayer-Kuckuk, "Matrix mineralization controls gene expression in osteoblastic cells," *Exp. Cell Res.*, vol. 372, no. 1, pp. 25–34, Nov. 2018.
[131] Bruker Method Note, "Bone mineral density (BMD) and tissue mineral density (TMD) calibration and measurement by micro-CT using Bruker-MicroCT CT-Analyser HU and BMD calibration in Bruker-MicroCT CT-analyser," p. 30, 2013.
[132] J. Oswald, R. Ailavajhala, and N. Pleshko, "Environmentally-Controlled Approaches for Near Infrared Spectroscopic Assessment of Cortical Bone Water," in *45th Annual Northeast Bioengineering Conference*, 2019.
[133] D. Pienkowski, T. M. Doers, M.-C. Monier-Faugere, Z. Geng, N. P. Camacho, A. L. Boskey, and H. H. Malluche, "Calcitonin Alters Bone Quality in Beagle Dogs," *J. Bone Miner. Res.*, vol. 12, no. 11, pp. 1936–1943, Nov. 1997.
[134] M. Unal and O. Akkus, "Raman spectral classification of mineral- and collagen-bound water's associations to elastic and post-yield mechanical properties of cortical bone," *Bone*, vol. 81, pp. 315–326, 2015.
[135] G. Cho, Y. Wu, and J. L. Ackerman, "Detection of Hydroxyl Ions in Bone Mineral by Solid-State NMR Spectroscopy," *Science (80-.).*, vol. 300, no. 5622, pp. 1123–1127, May 2003.
[136] J. D. Pasteris, B. Wopenka, J. J. Freeman, K. Rogers, E. Valsami-Jones, J. A. M. van der Houwen, and M. J. Silva, "Lack of OH in nanocrystalline apatite as a function of degree of atomic order: implications for bone and biomaterials," *Biomaterials*, vol. 25, no. 2, pp. 229–238, Jan. 2004.
[137] E. A. Zimmermann, E. Schaible, H. Bale, H. D. Barth, S. Y. Tang, P. Reichert, B. Busse, T. Alliston, J. W. Ager, and R. O. Ritchie, "Age-related changes in the plasticity and toughness of human cortical bone at multiple length scales.," *Proc. Natl. Acad. Sci. U. S. A.*, vol. 108, no. 35, pp. 14416–21, Aug. 2011.
[138] O. Demontiero, C. Vidal, and G. Duque, "Aging and bone loss: new insights for the clinician.," *Ther. Adv. Musculoskelet. Dis.*, vol. 4, no. 2, pp. 61–76, Apr. 2012.
[139] C. Ruckebusch, L. Duponchel, J.-P. Huvenne, and J. Saurina, "Multivariate curve resolution of step-scan FTIR spectral data," *Vib. Spectrosc.*, vol. 35, no. 1–2, pp. 21–26, Jun. 2004.
[140] E. Widjaja and M. Garland, "Pure component spectral reconstruction from mixture data using SVD, global entropy minimization, and simulated annealing. Numerical investigations of admissible objective functions using a synthetic 7-species data set," *J. Comput. Chem.*, vol. 23, no. 9, pp. 911–919, Jul. 2002.

[141] W. C. Bae, P. C. Chen, C. B. Chung, K. Masuda, D. D'Lima, and J. Du, "Quantitative Ultrashort Echo Time (UTE) MRI of Human Cortical Bone: Correlation with Porosity and Biomechanical Properties," *J Bone Min. Res*, vol. 27, no. 4, pp. 848–857, 2012.

APPENDIX

Micro-CT images of tibial cross-sections acquired from SkyScan 1172 equipped with a Hamamatsu C9300 11Mp camera using the double-side and oversize sample options. The parameters used for micro-CT images collection were as follows: Source voltage, 62 kV; source current, 131 mA; 9.89µ pixel resolution, rotation step was 0.2°, 5 frames averaging, and random movement compensation was 10. The acquisition time for each sample was ~10 hours. Images were acquired from 10% distal end of tibial cross-sections from 15 donors with ages ranging from 33-88 years old (Fig. 27). The images were reconstructed using a ring artifact correction of 10, and a beam hardening correction of 60% was applied uniformly to all samples. Subsequently samples were rotated using cortical bone was selected as the volume of interest (VOI) using a global threshold of 80 Hounsfield units (HU) for all the samples. The binarized images were used for porosity analysis using custom processing algorithm on SkyScan CT Analyzer software (CTAn). Cortical bone TMD calibrated to known standards of CaHA of 0.25 and 0.75 g/ cm-3 4 mm in diameter) were acquired from micro-CT images [131]. The calibration values were generated using custom processing algorithm on CTAn. Table 5 consists of the correlation between NIR inverted second derivative peak height ratios of water/ matrix in hydrated and dehydrated tissues to structural properties acquired from micro-CT.

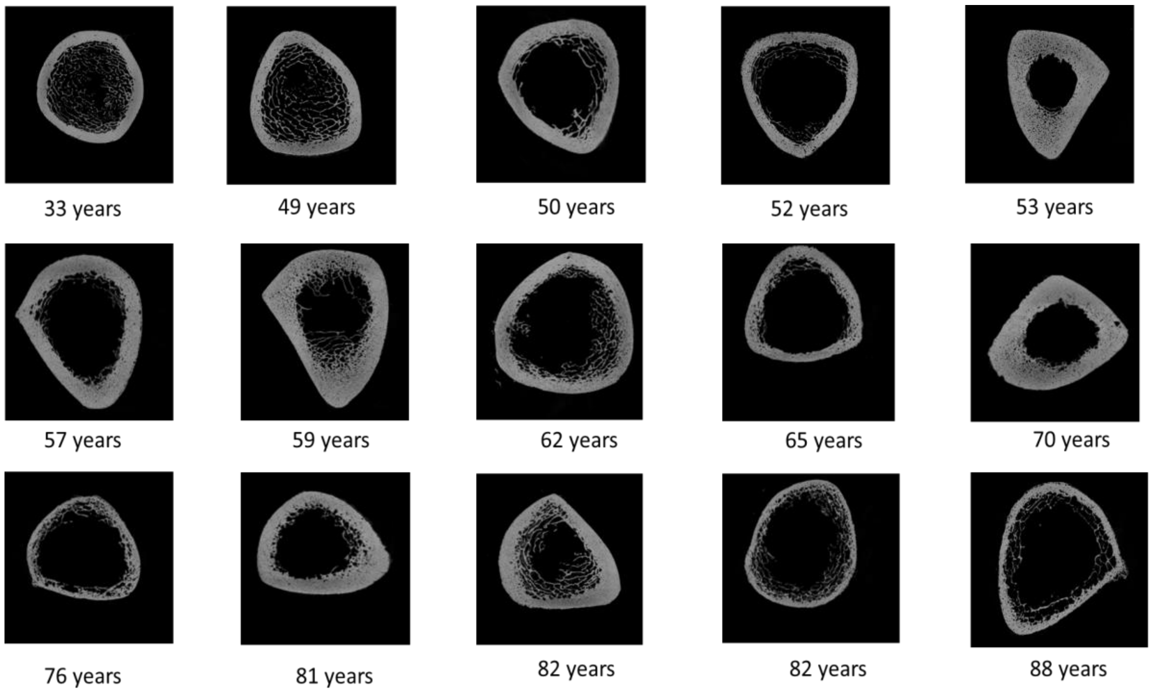

Figure 27: Micro-CT images from tibial cross-sections of donors from age 33-88 years old.

Table 5: Correlation of NIR inverted second derivative peak height intensities to structural properties.

Males +Females	**NIR Ratio: 5200/4608_Hydrated tissues**	**NIR Ratio: 5200/6688_Hydrated tissues**	**NIR Ratio: 7000/4608_Hydrated tissues**	**NIR Ratio: 7000/6688_Hydrated tissues**
Age of Donors	R= -0.46, p= 0.06	R= -0.41,p= 0.10	R= 0.24,p= 0.35	R = 0.22,p= 0.39
Porosity	R= -0.20, p= 0.44	R= -0.06,p=0.81	R=-0.19,p= 0.46	R=-0.17,p= 0.51
TMD	R=-0.62, p= 0.01	R=-0.65,p= 0.01	R=-0.04,p= 0.87	R=-0.07,p= 0.78
Males + Females	**NIR Ratio: 5200/4608_Dehydrated tissues**	**NIR Ratio: 5200/6688_Dehydrated tissues**	**NIR Ratio: 7000/4608_Dehydrated tissues**	**NIR Ratio: 7000/6688_Dehydrated tissues**
Age of Donors	R=0.08,p= 0.76	R=0.04,p= 0.11	R=0.16,p= 0.53	R=0.14,p= 0.59
Porosity	R=-0.42,p=0.09	R= -0.32,p= 0.21	R=-0.51,p= 0.036	R=-0.44,p= 0.07
TMD	R=-0.10,p= 0.70	R=-0.11,p=0.67	R=0.34,p= 0.18	R=0.19,p=0.46
Females	**NIR Ratio: 5200/4608_Hydrated tissues**	**NIR Ratio: 5200/6688_Hydrated tissues**	**NIR Ratio: 7000/4608_Hydrated tissues**	**NIR Ratio: 7000/6688_Hydrated tissues**
Age of Donors	R=-0.51,p= 0.30	R=-0.42,p=0.40	R=0.30,p= 0.56	R=0.29,p= 0.57
Porosity	R=-0.09,p= 0.86	R=-0.09,p= 0.86	R=-0.09,p= 0.86	R=0.59,p= 0.21
TMD	R=-0.72,p=0.10	R=-0.68,p= 0.13	R=0.11,p= 0.83	R=0.09,p= 0.86
Females	**NIR Ratio: 5200/4608_Dehydrated tissues**	**NIR Ratio: 5200/6688_Dehydrated tissues**	**NIR Ratio: 7000/4608_Dehydrated tissues**	**NIR Ratio: 7000/6688_Dehydrated tissues**
Age of Donors	R=0.63,p= 0.18	R=0.63,p= 0.18	R=0.39,p= 0.44	R=0.48,p= 0.33
Porosity	R=-0.23,p= 0.66	R=-0.20,p= 0.70	R=-0.66,p= 0.15	R= -0.57,p= 0.23
TMD	R=0.69,p= 0.13	R=0.65,p= 0.16	R=0.71,p= 0.11	R=0.73,p= 0.09
Males	**NIR Ratio: 5200/4608_Hydrated tissues**	**NIR Ratio: 5200/6688_Hydrated tissues**	**NIR Ratio: 7000/4608_Hydrated tissues**	**NIR Ratio: 7000/6688_Hydrated tissues**
Age of Donors	R= -0.45,p= 0.16	R= -0.39,p= 0.23	R= -0.44,p= 0.18	R= -0.46,p= 0.15
Porosity	R=-0.29,p= 0.38	R= -0.10,p= 0.76	R= -0.44,p= 0.18	R= -0.26,p= 0.44
TMD	R= -0.29,p= 0.38	R= -0.60,p= 0.05	R= -0.22,p= 0.51	R= -0.61,p= 0.04
Males	**NIR Ratio: 5200/4608_Dehydrated tissues**	**NIR Ratio: 5200/6688_Dehydrated tissues**	**NIR Ratio: 7000/4608_Dehydrated tissues**	**NIR Ratio: 7000/6688_Dehydrated tissues**
Age of Donors	R= -0.42,p= 0.19	R= -0.43,p= 0.19	R= -0.25,p= 0.45	R= -0.37,p= 0.26
Porosity	R= -0.38,p= 0.24	R= -0.37,p= 0.26	R= -0.41,p= 0.21	R= -0.42,p= 0.19
TMD	R= -0.37,p= 0.26	R= -0.41,p= 0.21	R= -0.03,p= 0.93	R= -0.28,p= 0.40